Article

Cell Systems

Higher-Order Interaction between Species Inhibits Bacterial Invasion of a Phototroph-Predator Microbial Community

Graphical Abstract

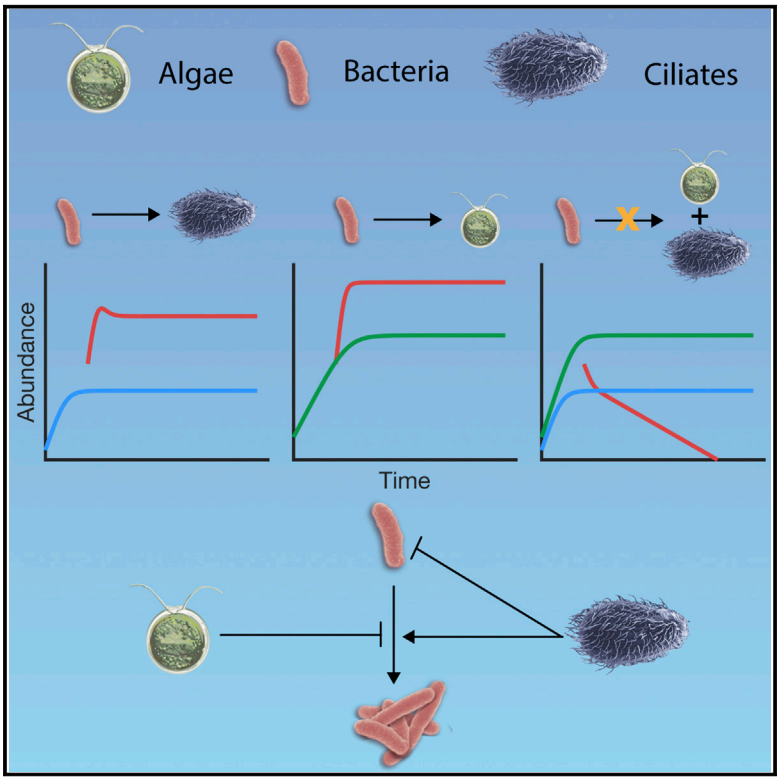

Authors

Harry Mickalide, Seppe Kuehn

Correspondence

seppe.kuehn@gmail.com

In Brief

Microbial communities inhabit nearly every niche on Earth. Frequent migration means that communities are invaded by new species. When and why an invader successfully establishes itself as a member of a community it invades is poorly understood. We study bacterial invasions of a microbial community containing a predator and a nutrient producer. We show that the presence of the producer enhances the ability of the predator to consume bacteria, making it more difficult for bacterial invasions to succeed.

Highlights

- Microbial communities can be invaded by new species changing their composition
- Measurements of bacterial invasions in an algae-predator microbial community
- Algae modify interaction between predator and bacteria changing invasion outcomes
- Theory shows apparent three-species (higher-order) interaction depends on model detail

Mickalide & Kuehn, 2019, Cell Systems *9*, 1–13
December 18, 2019
https://doi.org/10.1016/j.cels.2019.11.004

CellPress

Please cite this article in press as: Mickalide and Kuehn, Higher-Order Interaction between Species Inhibits Bacterial Invasion of a Phototroph-Predator Microbial Community, Cell Systems (2019), https://doi.org/10.1016/j.cels.2019.11.004

Cell Systems
Article

Higher-Order Interaction between Species Inhibits Bacterial Invasion of a Phototroph-Predator Microbial Community

Harry Mickalide[1,2] and Seppe Kuehn[1,2,3,4,*]
[1]Department of Physics, University of Illinois at Urbana-Champaign, Urbana, IL 61801, USA
[2]Center for the Physics of Living Cells, University of Illinois at Urbana-Champaign, Urbana, IL 61801, USA
[3]Carl R. Woese Institute for Genomic Biology, University of Illinois at Urbana-Champaign, Urbana, IL 61801, USA
[4]Lead Contact
*Correspondence: seppe.kuehn@gmail.com
https://doi.org/10.1016/j.cels.2019.11.004

SUMMARY

The composition of an ecosystem is thought to be important for determining its resistance to invasion. Studies of natural ecosystems, from plant to microbial communities, have found that more diverse communities are more resistant to invasion. In some cases, more diverse communities resist invasion by more completely consuming the resources necessary for the invader. We show that *Escherichia coli* can successfully invade cultures of the alga *Chlamydomonas reinhardtii* (phototroph) or the ciliate *Tetrahymena thermophila* (predator) but cannot invade a community where both are present. The invasion resistance of the algae-ciliate community arises from a higher-order interaction between species (interaction modification) that is unrelated to resource consumption. We show that the mode of this interaction is the algal inhibition of bacterial aggregation, which leaves bacteria vulnerable to predation. This mode requires both the algae and the ciliate to be present and provides an example of invasion resistance through an interaction modification.

INTRODUCTION

Microbial communities inhabit nearly every niche on Earth, from soils and oceans to plant and animal hosts. Rapid dispersal of microbes from one environmental context to another (Bovallius et al., 1978; Stocker et al., 2008) means that these communities are constantly confronted with invaders. Therefore, understanding the mechanisms of invasion resistance in microbial communities is central to understanding the structure of those communities in nature. Moreover, a fundamental understanding of microbial community invasion dynamics is necessary for successfully designing industrial processes such as algal biofuel production (Letcher et al., 2013) or controlling harmful invasions in nature such as blooms (Chambouvet et al., 2008).

Our current understanding of when and why some invasions succeed and others fail is grounded in the idea that an invader must either outcompete an existing community member for an available resource (dominance) or consume a resource that is not already being consumed by the community (complementarity) (Elton, 1958). Dominance and complementarity have successfully explained the outcome of invasions in a wide range of studies. For example, in laboratory populations of *Pseudomonas fluorescens*, more diverse communities resisted invasion more effectively by more completely occupying the available niches (Hodgson et al., 2002). Qualitatively similar results were observed for *E. coli* invasions of soil communities (van Elsas et al., 2012), wherein diversity of, and resource consumption by, the community were positively correlated with invasion resistance. Similarly, studies of plant root bacterial communities demonstrated that community resource competition networks could reliably predict the outcome of invasions both *in vitro* and in tomato plant root communities (Wei et al., 2015). Similar results have been found for plant communities on a larger spatial scale (Tilman, 1997).

Recently, theoretical work using consumer-resource models has extended this intuition and suggested that the emergent resource consumption and exchange in cross-feeding communities can be understood as a community-level fitness, which provides cohesiveness and therefore invasion resistance (Tikhonov, 2016). Experimental efforts suggest that this picture can capture some features of experimental invasions in bacterial communities (Lu et al., 2019). Collectively, this work shows that substantial insight into invasion dynamics can come from understanding resource dynamics during an invasion process.

However, in nearly all microbial communities, interactions exist that are not directly mediated by resources: for example, interactions mediated by the secretion of antibiotics (Vetsigian et al., 2011) or predation by protists (Jost et al., 1973) or phage (Rodriguez-Brito et al., 2010). Some studies have been undertaken to examine the role these types of interactions play in determining the fate of invading species (Ravva et al., 2013); however, as recently pointed out by Mallon et al. (2015), it remains an outstanding question how interactions that are not mediated by resources, such as predation, affect community invasion dynamics.

Here, we use a model microbial community to study invasion dynamics in the presence of predation. Microbial communities in freshwater lakes and nearby saturated soils are occupied by primary producers who fix inorganic carbon, metabolically

flexible heterotrophic bacteria who decompose organic matter, and predators who unlock nutrients held in biomass (Kirchman, 2012). To study this canonical natural community, we use a three-species model microbial ecosystem comprising the alga *Chlamydomonas reinhardtii*, which acts as a primary producer and is an endemic phototroph in soils and freshwater (Sack et al., 1994), the bacterium *Escherichia coli*, which acts as a decomposer and is common in soils (Ishii et al., 2006), and the ciliate *Tetrahymena thermophila*, which dwells in freshwater and preys on *E. coli*. We refer to this model ecosystem as the "ABC" community for algae, bacteria, and ciliates. The ABC community has been studied previously as a model self-sustaining closed microbial ecosystem (Frentz et al., 2015; Hekstra and Leibler, 2012; Kawabata et al., 1995). Recent work has shown that long-term abundance dynamics in closed ABC ecosystems are complex and deterministic on timescales of months, exhibiting rich spatiotemporal and phenotypic dynamics (Frentz et al., 2015). The fact that the composition of the ABC community reflects the structure of some natural communities and that quantitative measurements are feasible make this a compelling model ecosystem for quantitative ecology (Widder et al., 2016).

Here, we show that when *E. coli* (B) is introduced into communities of *C. reinhardtii* (A) and *T. thermophila* (C), A modifies the interaction between B and C, resulting in failed invasions (see Box 1). When B invades C alone, B aggregates to avoid predation by C and successfully grows to a high density. Similarly, when B invades A alone, A may stall the invasion of B, but B can still successfully invade and grow to a high density. In contrast, when B is introduced into a community of C and high-density A ($> 5 \times 10^4 mL^{-1}$), B always fails to invade. We demonstrate that nutrient competition is not responsible for the invasion dynamics we observe. Instead, we find that A inhibits aggregation of B, resulting in increased predation pressure on B by C and therefore a decline in B abundances. We construct a simple model of the population dynamics in this microbial community that faithfully recapitulates the invasion of B in communities of A and/or C. We then use the model to predict the abundance dynamics of all three species as a function of light level where we find higher light levels result in lower B abundances because of increased A densities. We confirm this prediction experimentally.

Our study provides a clear example of interaction modification (Billick and Case, 1994; Wootton, 1994), whereby one species (A) modifies the interaction between two other species (B and C). In ecology, interaction modifications are often termed "higher-order interactions" because describing them mathematically by modeling the impact of each species' abundance on those of other species (e.g., a Lotka-Volterra formalism) requires a term that is the product of all three species abundances (Billick and Case, 1994). We show that describing the abundance dynamics in our community using a Lotka-Volterra formalism indeed requires such a higher-order term. As a result, we refer to interaction modification as a "higher-order interaction." We go on to show that a higher-order term (product of three species' abundances) is not necessary when we explicitly model the aggregation of the bacteria (Box 1). Therefore, the higher-order interaction we observe is fundamentally distinct from higher-order effects in physical systems that cannot be decomposed into pairwise terms irrespective of the level of description. Quite to the contrary, our results show that higher-order interactions in ecosystems can be accounted for quantitatively with pairwise terms when the mathematical description of the system includes the necessary microscopic details.

RESULTS

We study the dynamics of the ABC community in batch culture conditions with the community open to gas exchange. Organisms are introduced at low initial densities into 30 mL of a freshwater mimic medium (Taub and Dollar, 1968) with undefined carbon and nitrogen sources (proteose peptone no. 3, see STAR Methods). To initiate an experiment, all three organisms are cultured axenically in their respective growth media. Cells are washed and then their densities are determined by flow cytometry. The communities are then constructed with known initial starting densities and maintained in custom culture devices, which control temperature via feedback to a Peltier element (30°C) and illumination via a light-emitting diode (LED) below the vial (Figure 1A).

Here, we present two types of experiments: coculture experiments and invasion experiments. Coculture refers to experiments in which all species are simultaneously introduced at low densities (5×10^2 mL^{-1} for A, 1×10^3 mL^{-1} for B, and 5×10^2 mL^{-1} for C) and in all possible monoculture, pair-culture, and tri-culture combinations. Initial densities were chosen to be low enough to require substantial growth of each species during the experiment but high enough to limit stochastic effects due to counting noise. A and C were started at lower densities than B because of their lower carrying capacities in these growth conditions. Invasion refers to experiments in which A and/or C is introduced at low density, allowed to grow for a fixed period of time (4 or 14 days), and then inoculated with B. In all experiments, abundance dynamics are followed approximately daily by sampling 500 μL of the community and performing flow cytometry measurements. Flow cytometry permits the quantification of abundances for A, B, and C by chlorophyll fluorescence, genetically encoded yellow fluorescent protein (YFP) fluorescence, and size, respectively (see STAR Methods). We performed a live-dead staining experiment to check that the cells counted with flow cytometry are alive (Figure S11). Because a significant number of B cells are present in aggregates, we developed an algorithm to estimate the number of cells in aggregates from the bacterial side-scatter signal. Previous studies have used side scatter as a proxy for aggregation as well (Hom and Murray, 2014). However, we note that the central findings of this study, where A modifies the interaction between B and C causing B invasions to fail in the presence of A and C (Figures 2 and 6), do not depend on correcting the bacterial counts for cells in aggregates (Figures S2 and S3).

We varied A's growth rate by performing experiments at two light levels: "low light" (average intensity of 1,600 Lux $\approx$ 23 μmol m^{-2} s^{-1}) or "high light" (average intensity of 4,200 Lux $\approx$ 60 μmol m^{-2} s^{-1}). The spectrum of the LEDs used here is shown in Figure S7. These light levels were chosen to assay the impact of changes in algal abundance dynamics on the community and resulted in approximately a factor two change in algal growth rates (Table S1). Light levels do not appear to impact the abundance dynamics of B or C

Box 1. Defining Higher-Order Interactions in the Context of a Mathematical Model of Algae-Bacteria-Ciliate Invasion Dynamics

To interrogate the nature of higher-order effects in the ABC community, we sought to model the invasion dynamics we observed. We first asked whether a model that describes abundance dynamics through effective interactions using a Lotka-Volterra formalism, but lacks mechanistic details of the interactions, is sufficient to explain our observations. We then interrogated a more detailed mechanistic model of the abundance dynamics. We found that the higher-order interaction manifests as a term that is the product of all three species abundances when mechanistic details of the interactions in the community are neglected. In contrast, a model incorporating the bacterial aggregation-deaggregation process contains no term that is the product of all three species abundances. Therefore, a model that includes mechanistic details accounts for the "higher-order interaction" without requiring a term that is the product of three species abundances.

We first sought a mathematical description of the invasion dynamics shown in Figure 2 using a Lotka-Volterra formalism, which captured the impact of the abundance of each species on the abundances of all other species. Theoretical studies of higher-order interactions in a Lotka-Volterra formalism include terms that are the product of more than two species' abundances (Bairey et al., 2016; Grilli et al., 2017). In fact, Billick and Case (1994) have proven that for any three species ecosystem exhibiting interaction modification, a model at the level of abundances of each species must include a higher-order term that is the product of three species' abundances (Billick and Case, 1994). As a result, the terms "higher-order interaction" and "interaction modification" are used interchangeably in the ecology literature.

To sharpen the theoretical claims from these studies, we asked whether the invasion dynamics in Figure 2 could be described using a Lotka-Volterra formalism at the level of abundances. We formulated a deterministic model describing the abundances of all three species that neglected both aggregation and substrates but instead only described abundance dynamics of each species. In this formalism, numerical simulations show that the following model qualitatively captures the invasion dynamics we observe experimentally (Figure S13).

$$\dot{x}_B = \left(r_B x_B - r_{AB}\frac{x_A x_B}{K_A} - r_{ABC}\frac{x_A x_C x_B}{K_{AC}}\right)\left(1 - \frac{x_B + \beta x_C}{K_B}\right). \quad \text{(Equation 1)}$$

$$\dot{x}_A = r_A x_A\left(1 - \frac{x_A}{K_A}\right). \quad \text{(Equation 2)}$$

$$\dot{x}_C = r_C x_C\left(1 - \frac{x_C}{K_C}\right). \quad \text{(Equation 3)}$$

Here, a dot denotes a derivative with respect to time, and x_i is the abundance of species i. r_i is the growth rate of species i, r_{AB} and r_{ABC} are interaction coefficients, and K_* are carrying capacities. Details of the model specification and parameters used are given in the STAR Methods and below. Briefly, the term $r_B x_B$ describes bacterial growth and the term $r_{AB} x_B x_A$ the inhibition of bacterial growth by algae. The higher-order term ($r_{ABC} x_A x_C x_B$) captures the interaction modification, and the term in the last set of parenthesis captures predation by C on B characterized by the constant β. The dynamics of x_A and x_C are modeled as logistic growth. For x_A in low light, we use lower growth rates (r_A) when x_B or x_C are present in the community (Table S1). The model neglects the decline in ciliate abundances towards the end of the experiment. We make this assumption because we find that ciliate dynamics are more sensitive to the culture from which the cells came than the light level or presence of A or B (Figure S6).

The model shown in Equations 1, 2, and 3 abstracts away mechanistic details of predation, aggregation, and nutrient consumption. As required by Billick and Case (1994), the model includes a term that is the product $x_A x_C x_B$. It is intuitive that this should be the case because any modification of the predation of B by C due to A cannot be accounted for by the simple predation term ($x_B x_C$) because such a term will exhibit no dependence on algal abundances.

Given the apparent importance of bacterial aggregation to the abundance dynamics we observe, we next asked whether a model that included aggregation could also capture the invasion dynamics in Figure 2. In this framework, we describe the abundance dynamics of the algae and ciliates, non-aggregated bacteria (x_B) as well as aggregated bacteria (A_B), and a single substrate consumed by x_B, which we denote S. The model takes the form:

$$\dot{x}_B = x_B\left(r_B - r_{AB}\frac{x_A}{K_A}\right)S - F x_B x_C - \alpha_1 x_B x_C + \alpha_2 A_B x_A. \quad \text{(Equation 4)}$$

$$\dot{A}_B = \alpha_1 x_B x_C - \alpha_2 A_B x_A. \quad \text{(Equation 5)}$$

$$\dot{x}_A = r_A x_A\left(1 - \frac{x_A}{K_A}\right). \quad \text{(Equation 6)}$$

(Continued on next page)

Box 1. *Continued*

$$\dot{x_C} = r_C x_C \left(1 - \frac{x_C}{K_C}\right). \quad \text{(Equation 7)}$$

$$\dot{S} = -\frac{1}{Y} x_B \left(r_B - r_{AB}\frac{x_A}{K_A}\right) S. \quad \text{(Equation 8)}$$

F is feeding rate, and α_1 and α_2 are aggregation and disaggregation rates of bacteria, respectively. Note that A_B do not grow (consume S) in this model. K_i captures the carrying capacity of species i, and Y is the yield of bacteria growing on S.

For a complete discussion of the modeling decisions we made, see the STAR Methods. Briefly, the first term in Equation 4 captures the fact that x_A only impacts the growth rate of x_B and not its final abundance. Substrate is considered explicitly to enforce the fact that x_B cannot recover from predation if it had already reached saturating density. The predation of x_B by x_C is linear in prey density, an assumption justified by the relatively low densities of bacteria in our experiment. We neglect growth of x_C on x_B because of the low yield of ciliates on bacteria and low densities of bacteria in our experiment. This assumption is supported by the data, which show no substantial difference in C densities with and without B (Figure S5). Aggregation terms are consistent with our observations in Figures 1 and 4. In this model, the mode by which bacteria ($x_B + A_B$) fail to invade communities of x_A and x_C is the disaggregation of A_B to x_B in a manner that is dependent on x_A density ($\alpha_2 A_B x_A$) and the subsequent predation of x_B by x_C ($F x_B x_C$).

r_{AB}, α_1, and α_2 were inferred from our data; F has been reported previously (Fenchel, 1980a; Hatzis et al., 1993, 1994); and all other parameters were measured in this study. r_{AB} must be on the order of r_B if we are to observe any substantial inhibition of x_B growth by x_A. α_1 can be constrained by a close examination of the BC pair-culture dynamics (Figure S12), and α_2 can be inferred from the relative abundances of all three species and A_B late in the experiment shown in Figure 5C (STAR Methods). With these parameter values (Table S3), we performed numerical integration of the model in Equations 4, 5, 6, 7, and 8 for the invasion experiments shown in Figure 2. The results are shown in Figure 2, alongside the measurements, where we plot total B abundances ($x_B + A_B$), A abundances (x_A), and C abundances (x_C).

We note that this model captures the basic features of the invasion experiments: (1) B successfully invades C cultures; (2) B densities in the presence of C are lower than those for B invasions of low-density A cultures (compare Figures 2A and 2B); (3) when B invades a high-density A culture, its growth rate is attenuated (Figures 2E, 2H, and 2J) but B eventually reaches high density ($>1 \times 10^6 \mathrm{mL}^{-1}$); (4) when B is introduced into an AC culture with high-density A, B declines in abundance continuously (Figures 2F, 2I, and 2K); and (5) when B is introduced into an AC culture with low-density A, B invades immediately but slowly declines in abundance over time (Figure 2C). Our deterministic model cannot capture the variability in outcomes of B invading A alone.

A comparison between the two models shows that the presence of a higher-order term depends on the level of description. Namely, a model that relies on effective interactions, rather than an explicit characterization of the mechanisms mediating those interactions, requires a higher-order term to correctly account for the interaction modification.

(Figure S5). Communities are mixed by a magnetic stirrer at a rate of 450 rpm and sampled through a sterile port.

Monoculture and Pair-Culture Dynamics

To begin, we measured monoculture and pair-culture dynamics in the high light condition (Figure 1). Pair-culture dynamics between A and B suggest limited impact of A on B growth rate or carrying capacity (Figures 1B, 1C, and 1F). Similarly, B does not measurably impact A growth rate or carrying capacity in this high light condition (see Table S1 for A growth rates).

In contrast, when B is pair cultured with C, we observe an approximately 10-fold reduction in the abundances of B relative to B monoculture. This reduction is expected because of the known predation of B by C. In these BC pair cultures, predation of B by C fails to drive B abundances below approximately 10^5 mL^{-1}, and at longer times B abundances increase (Figure 1H). Previous measurements of ciliate feeding rates (Fenchel, 1980a), however, suggest that at these densities, C should be able consume most of the B present (STAR Methods). We propose that the ability of B to sustain comparatively high densities in the presence of C is driven by B aggregation (Blom et al., 2010). Bacterial aggregation is a common defense against predation because of the fact that the oral apparatus of the ciliates has a limited range of prey sizes it can accommodate (Corno and Jürgens, 2006; Fenchel, 1980b). Sufficiently large aggregates of B cannot be consumed by C. Indeed, we show that B aggregates much more in the presence of C than in monoculture (Figure 1E). B aggregation was quantified by side-scatter measurements (Figure S1). We conclude that B abundances are reduced by predation, but the impact of predation is limited by aggregation. We also note that C abundances are not substantially impacted by the presence of B. This fact is in accordance with the low yield of ciliates on bacteria as previous work suggests 1×10^3 to 4×10^4 bacteria are required to produce a single ciliate (see STAR Methods) (Seto and Tazaki, 1971).

Finally, when A and C are pair cultured, the dynamics of C is minimally impacted relative to C monoculture (Figures 1D and 1G). Taken together, Figure 1 suggests that the dominant interaction in the ABC community is predation of B by C, whereas interactions between A and B or A and C are limited.

Bacterial Invasions of Ciliates

We studied the dynamics of B invading C. We introduced B at a density of $\sim 1 \times 10^4$ mL^{-1} into established cultures of C 4 and 14 days after the initiation of C cultures (Figures 2A, 2D, and 2G). We find that irrespective of the timing of the introduction

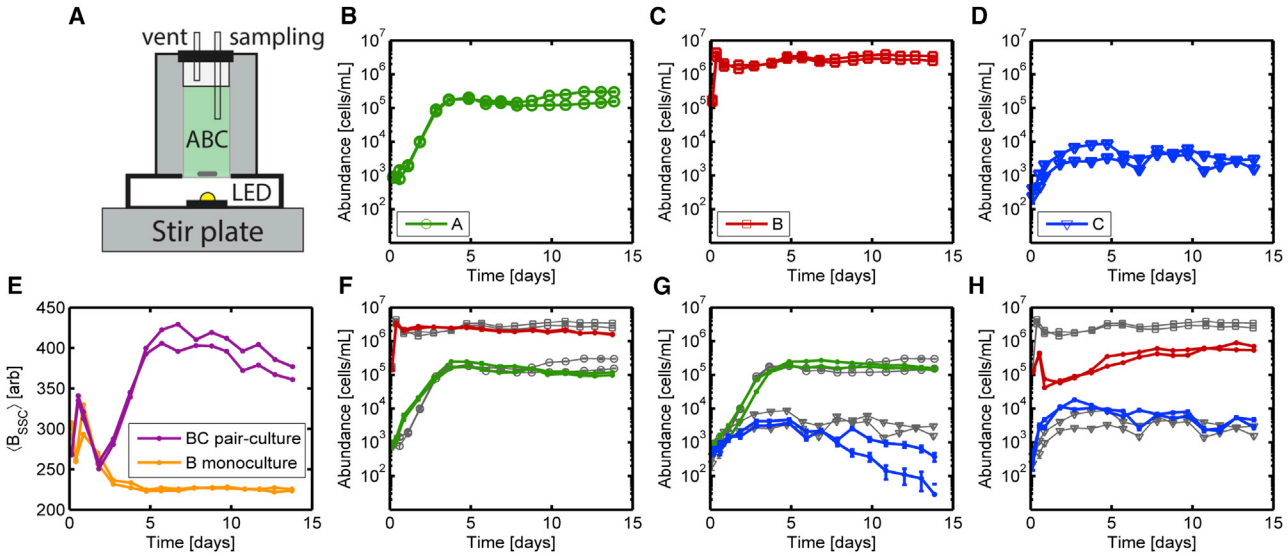

Figure 1. Monoculture and Pair-Culture Dynamics with Algae, Bacteria, and Ciliates

(A) A schematic of the custom culture devices used in this study.

(B–D) Abundance dynamics plotted for monocultures of algae (A, circles), bacteria (B, squares), and ciliates (C, triangles), respectively, at 4,200 Lux (high light).

(E) Mean side-scatter signal of B as a function of time in B monoculture and BC pair culture. Data from some of these coculture experiments were used to perform live-dead staining experiments (see Figure S11) and calculate A and C growth rates (see Table S1).

(F–H) Abundance dynamics for AB, AC, and BC pair culture, respectively, also at 4,200 Lux. Gray traces are for monocultures of A, B, or C with the markers corresponding to (B)–(D). For each experiment, there are two independent replicates. Abundances are measured via flow cytometry. Error bars are computed as described in the STAR Methods. For time points where error bars are not visible, errors are smaller than the size of the points. B abundances are reported as the total number of cells including planktonic cells and cells in aggregates (see Figure S1).

of B or the light levels, B successfully grows to high densities ($> 1 \times 10^5$ mL^{-1}). As in BC pair culture (Figure 1E), side-scatter intensity for B in invasion experiments confirms B aggregation in the presence of C (Figure S4). For the purposes of discussion, we define a successful B invasion as one in which B abundances exceed 7×10^4 mL^{-1} at the end of the experiment or, in the case of Figure S2C, when B abundances rise above 7×10^4 mL^{-1} and then remain high for several days.

Bacterial Invasions of Algae

Next, we studied the dynamics of B invading A (Figures 2B, 2E, 2H, and 2J). If A densities are low at the time of B invasion, then B successfully grows to a high density (Figure 2B). When A densities are high at the time of B invasion, B exhibits either very slow growth eventually reaching high densities more than 7 days after introduction or crashes to low densities over a period of more than 5 days (Figure 2E). In these experiments, the ultimate outcome of B invasions is variable, with some succeeding and others failing, even between two identically prepared replicates (Figures 2H and 2J). We find that inhibition of B growth by A only occurs when A is at a high density and that the inhibition occurs both at low and high light levels (Figures 2E, 2H, and 2J). When A abundances are high at the time of B introduction, B eventually reaches a high density ($>7 \times 10^4$ mL^{-1}) 50% of the time (5 of 10 invasion experiments, Figures 2E, 2H, 2J, and S8C). However, when A densities are low at the time of B introduction, B grows to a high density immediately in every replicate (8 of 8 experiments, Figures 1F, 2B, S8A, and S8B). Note that the inhibitory interaction between A and B is only apparent when B has not reached stationary phase. If B reaches stationary phase before A abundances reach roughly 5×10^4 mL^{-1}, we observe no inhibition of B by A, not even once A abundances exceed 5 × 104 mL−1 later in the experiment (compare Figures 1C and 1F).

To more thoroughly study the dependence of B invasion success on A density, we performed a set of invasion experiments where B was introduced into A cultures at $t = 0$ (pair-culture experiment), 1, 3, and 4 days, all at high light (4,200 Lux) (Figures S8A–S8D). We found that for those A cultures that exceeded a density of 5×10^4 mL^{-1} at the time of B introduction, B growth was inhibited. We conclude that a threshold on the abundance of A determines the outcome of B invasions (this threshold is shown as a green line in Figure 2 when A is present).

We next showed that resource competition is not the mechanism by which A inhibits B growth. We harvested spent media from an AB invasion experiment at several time points (Figure 2E pink traces, Figure 3C). We filtered out both A and B and inoculated fresh B cells at a low density into this spent media. We then incubated these cultures and assayed B carrying capacity on the spent media by flow cytometry. B was able to grow to a high density ($> 10^5$ mL^{-1}) on spent media harvested before $\sim t = 15$ days (Figures 3C and 3D). For spent media harvested after $\sim t = 15$ days (when B finally grows to a high density), B can no longer grow to a high density on the spent media. This result shows that consumable nutrients exist for B, even while B's growth is being inhibited by A. High-density populations of A do not compete with B for these nutrients but do limit the ability of B to consume them.

Algal Inhibition of Bacterial Growth

We undertook a series of experiments to better understand the mechanism by which A inhibits B growth. We found that the

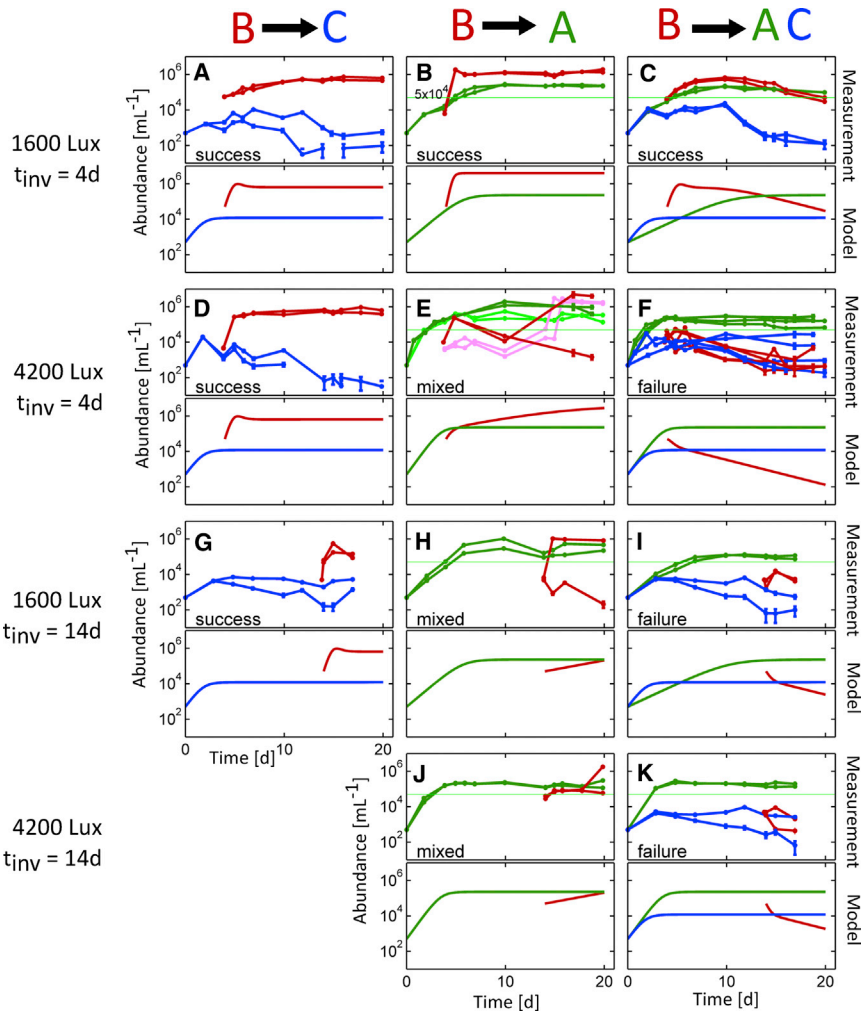

Figure 2. Measurement and Modeling of Bacterial Invasion Dynamics

Measurements of abundance dynamics during invasions are shown with numerical simulations of a mathematical model of ABC interactions. As labeled on the right, panels are paired, with measurements (lines + markers) in the top panel and simulations (curves) on the bottom. A, B, and C abundances are shown in green, red, and blue, respectively. B invasions of C (left column), A (middle column), or AC (right column) occurred in either 1,600 Lux (low light) or 4,200 Lux (high light) at day 4 or 14 as indicated for each row on the left. In each condition (community composition, light intensity, and invasion time), at least two replicate communities were measured. Labels in each panel, that is, "success," "failure," or "mixed," indicate the classification of the outcome of bacterial invasion, with success defined as B exceeding a density of $7 \times 10^4 mL^{-1}$ for an extended period of time. The horizontal green line at $5 \times 10^4 mL^{-1}$ indicates a threshold on A that was determined in control experiments (Figures S8A–S8D). When A exceeds this threshold, B invasions can be inhibited. In (E), pink traces for B and light green traces for A denote experiments in which spent media measurements were performed (Figure 3C). Abundances are measured via flow cytometry. Error bars are computed as described in the STAR Methods. For time points where error bars are not visible, errors are smaller than the size of the points. For time points where C abundances are not shown, no ciliates were detected. B abundances are reported as the total number of cells including planktonic cells and cells in aggregates (see Figure S1). Simulation of the model is described in the text and STAR Methods. Abundance dynamics of A (x_A), B (x_B+A_B), and C (x_C) are shown in green, red, and blue, respectively. The model is given by Equations 4, 5, 6, 7, and 8. Parameter values are given in Table S3.
See also Table S2 and Figures S5, S12, and S13. For a complete discussion of the model, see Box 1.

inhibition of B growth by A requires illumination and that the presence of A alone, in the absence of light, is not sufficient to inhibit B growth (Figure S8F). Literature on algae-bacteria interactions suggests that reactive oxygen species may be responsible for bacterial growth inhibition (Morris et al., 2011; Wojtaszek, 1997), but we showed conclusively that A was not producing sufficient H_2O_2 to limit B growth (STAR Methods). We found that the role of light intensity in the inhibition of B growth was dependent on the growth history of A (e.g., Figure S8J). Furthermore, we considered the hypothesis that increased cell-to-cell contact due to the higher density of A could be responsible for the inhibition of B growth by A. We estimated the frequency of B collisions with A to be high even at low A density, and so we expect that an increase in physical contact between A and B due to higher A density would not be responsible for the inhibition (STAR Methods). Additionally, detailed analysis of our flow cytometry data showed that A and B stick to each other, but the rate is low (~5%) and does not change significantly between inhibited and successful invasions (Figure S10). As a final check, we confirmed that successful invasions were not a case of A detritus being misclassified as B (STAR Methods).

Irrespective of the molecular mechanism of the antagonistic interaction between A and B, it is clear that the inhibition of B requires high-density A, light, and a B population that has not reached stationary phase. Finally, the variable outcomes for B invading A are in contrast to the reproducible dynamics observed in Figure 1 and in previous studies (Frentz et al., 2015), suggesting that there may be stochastic processes at the single-cell level that are responsible for the inhibition or that the system is highly susceptible to small experimental variations near the transition between B inhibition and B growth. We now turn to the central topic of the present study, the invasion of B into AC communities.

Bacteria Fail to Invade Algae-Ciliate Communities When Algal Densities Are High

Next, we performed B invasions of AC cultures (Figures 2C, 2F, 2I, and 2K). We found that in every single case where C is present and A density exceeds 5×10^4 mL^{-1} at the time of

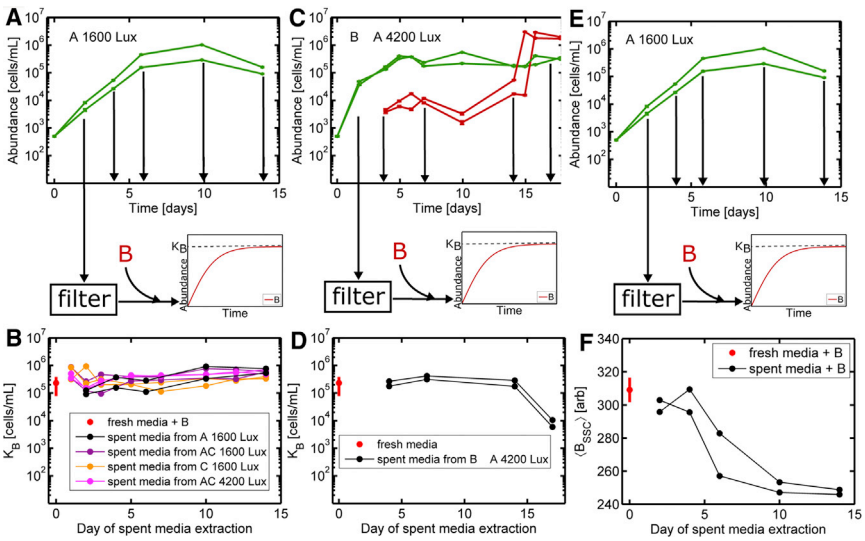

Figure 3. Spent Media Experiments Reveal Absence of Nutrient Competition and Presence of Disaggregating Effect of Algae on Bacteria

(A) Abundance plotted versus time for two replicates of an algae monoculture at 1,600 Lux (low light). Black arrows indicate the time points when media is extracted and filtered. Bacteria are then grown on this spent media in a microtiter plate until it reaches saturation. The saturating density K_B is measured via flow cytometry. This experiment is also performed on a 1,600 Lux C monoculture, 1,600 Lux AC coculture, and 4,200 Lux AC coculture.

(B) K_B is plotted for all the conditions. The x axis indicates the day of extraction of spent media.

(C) The same spent media extraction experiment is performed on a monoculture of algae that is invaded with bacteria. This means that the spent media taken from this culture has already been exposed to bacteria.

(D) K_B plotted versus day of spent media extraction for the experiment in (B).

(E and F) (E) Reproduction of (A). (F) Mean side-scatter of the bacteria after they reach K_B is plotted versus time of spent media extraction from cultures in (E). The point at time zero represents the mean side scatter of bacteria that were grown on fresh media.

See Figures S8, S10, and S9.

B introduction, B fails to invade and ultimately declines to very low densities (Figures 2F, 2I, and 2K). This result stands in contrast to B's successful invasions of A or C alone. When B is introduced into an AC community with a low A density ($<5 \times 10^4$ mL^{-1}), B grows to a high density and then slowly declines in abundance later in the experiment (Figure 2C). We conclude that if C is present and A is at a high density at the time of B introduction, B cannot proliferate and ultimately declines to low abundance. B's failure to invade AC cultures is the main finding of this study.

One possible explanation for this finding is that AC communities with high A densities have exhausted a critical nutrient for B growth. Spent media experiments again show this not to be the case. We performed a series of spent media experiments where communities with A, C, or A and C were grown, samples were harvested, and then all cells were removed by filtration (Figures 3A and 3B). B was then inoculated into this spent media and grown to saturation in a 96-well plate where its abundance was assayed by flow cytometry. This measurement captures the carrying capacity of bacteria on the spent media. We find that B is able to grow on the spent media of A, C, and AC communities to a saturating density that is indistinguishable from growth on fresh media, irrespective of the time at which the spent media was taken (Figure 3B). This result rules out the hypothesis that nutrient competition accounts for any of the invasion outcomes in Figure 2.

Because pH is known to play an important role in mediating interactions in microbial communities (Fierer and Jackson, 2006), we also considered the role of pH in determining the outcome of B invasions. For most of the experiments shown in Figure 2, we measured pH at the end of the experiment (Table S2). The final pH varied between about 6.5 and 8.9, but we observed no clear correlation between the final pH and the success or failure of the B invasion. For example, at high light AC t_{inv} = 4 days, B fails to invade, and the final pH is slightly acidic (~6.6). Conversely, even in the low light AC t_{inv} = 14 days, B fails to invade, and the final pH is ~8.25.

The results of Figure 2 suggest that a higher-order effect, unexpected from pairwise interactions, governs the outcome of B invasions of AC communities. Only when A and C are both present do B invasions reliably fail. Next, we sought to understand the mode of this effect through experiments, and more formally through modeling (see Box 1 and STAR Methods).

Algae Enhance Ciliate Predation of Bacteria in a Density-Dependent Fashion by Inhibiting Bacterial Aggregation

We propose that a higher-order interaction is responsible for the fact that B cannot invade an AC community when A abundances exceed 5×10^4mL^{-1}: high-density A induces B to remain in a planktonic (single-celled) state, robbing B of aggregation, its primary defense mechanism against predation by ciliates (Figure 1E). The mechanism we propose here is consistent with what ecologists have previously called an interaction modification (Wootton, 1994).

First, we show that B aggregation is inhibited by high-density A. Note that as bacteria grow in monoculture, they initially aggregate and then ultimately disaggregate (Figure 1E, orange traces). This non-monotonic change in aggregation is potentially due to substrate-level-dependent aggregation rates observed previously (Merritt and Kuehn, 2016, 2018). When A and B are grown in pair culture, the aggregation and subsequent dispersal of B is nearly identical to what we observe in B monocultures (compare red traces in Figure 4E to orange traces in Figure 1E). Similar B aggregation dynamics are observed when B invades a low-density A culture (Figures 4B and 4E). However, when B invades at day 4 into a high-light (4,200 Lux) A culture that has reached 1×10^5mL^{-1}, B does not grow immediately (Figure 4C), and for the duration of this growth inhibition, their aggregation is inhibited (Figure 4E, black traces). Only once the inhibitory effects

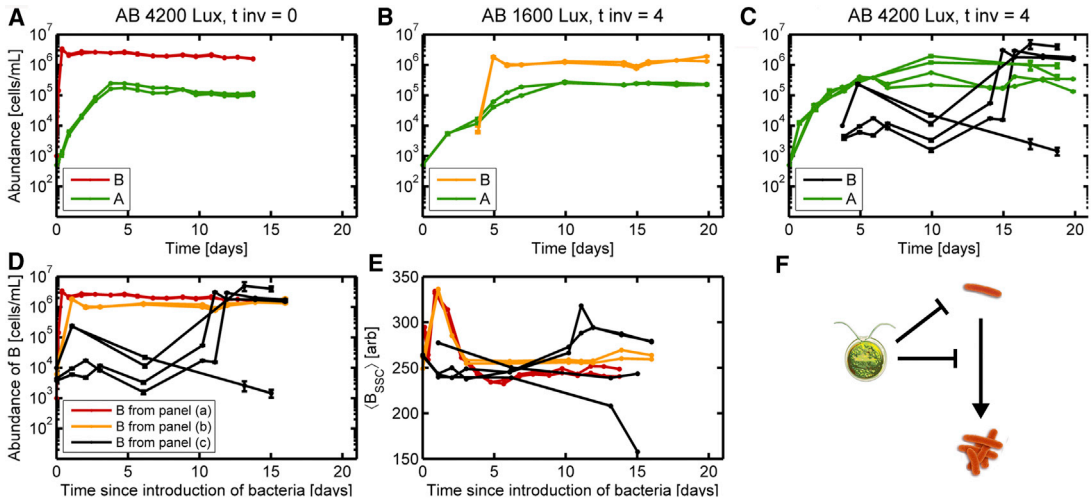

Figure 4. Algae Suppresses Bacterial Aggregation

(A–C) A abundances are shown in green. Color of B abundance trace varies in (A)–(C) as indicated in the legends. (A) Abundance dynamics for two replicates of a high light (4,200 Lux) AB pair culture (t_{inv} = 0 days). (B) Abundance dynamics for two replicates of a B invasion on A in low light (1,600 Lux) with t_{inv} = 4 days. A density is ~1 × 10^4mL^{-1} at the time of B introduction. (C) Abundance dynamics for four replicates of a B invasion on A in high light (4,200 Lux) with t_{inv} = 4 days; A density is > 1 × 10^5mL^{-1} at the time of B introduction. Abundances are measured via flow cytometry. Error bars are computed as described in the STAR Methods. For time points where error bars are not visible, errors are smaller than the size of the points. B abundances are reported as the total number of cells including planktonic cells and cells in aggregates (see Figure S1).

(D) Overlay of B abundances from (A), (B), and (C), translated so that t = 0 corresponds to the time of B introduction.

(E) Overlay of the mean side-scatter signal of B, translated so that t = 0 corresponds to the time of B introduction. The low side-scatter signal at the final time point in one of the black traces arises from a small number (20) of counts. Colors of traces in (D) and (E) correspond to (A)–(C).

(F) Diagram of interactions for A and B. Blunt arrowhead from A to B indicates the inhibition of B growth by A. Blunt arrow from A to the transition between planktonic and aggregated B indicate the inhibition of B aggregation by A. (A) is reproduced from Figure 1F, and (B) and (C) are reproduced from Figures 2B and 2E. For more data on interactions between A and B, see Figures S8 and S10.

of the algae are overcome by B after 10 days can B grow and aggregate. We conclude that algae inhibit bacterial aggregation in a manner that depends on the density of algae.

We investigated the inhibition of B aggregation by A further by examining the effect of A spent media on the ability of B to aggregate (Figure 3F). Using data from the previously described spent medium experiment, we examined the aggregation state of B (using mean side scatter as a proxy) as a function of the time at which the spent media was extracted from the growing A culture. We find an inverse relationship between the extraction time of spent media and level of B aggregation when grown on that spent media. The fact that A is not physically present in the spent media suggests that its ability to inhibit B aggregation is mediated by a chemical rather than a physical interaction. Interestingly, while spent media from an A monoculture disaggregates B, it does not inhibit growth of B. This result indicates that aggregation is not necessary for B to grow in this media. The independence of aggregation and growth is supported by the fact that a B mutant deficient in aggregation (Δ*csgA*) grows in monoculture on this media without aggregating (Figure S4L). Our observation that A disaggregates B is qualitatively consistent with observations that *Chlamydomonas* can secrete signaling molecules such as auto-inducers, which can interfere with biofilm formation (Teplitski et al., 2004).

C has the opposite effect on B in that it induces B to aggregate (Figures 1E and S4). In all cases where only B and C are present, aggregation of B greatly exceeds that in B monoculture or AB pair culture. We conclude that A and C have opposing effects on the aggregation state of B, with A inhibiting and C enhancing aggregation.

We hypothesize that the failure of B to invade a culture of C and high-density A (Figure 5C) is due to A inhibiting B aggregation and subsequently increasing the predation pressure of C on B. Under this hypothesis, we expect that when B fails to invade an AC community, B will have failed to aggregate, and this is what we observe (Figure 5E). Conversely, when B successfully invades an AC community (which occurs when A is at a low density at the time of B introduction), B aggregates effectively as we expect, thus evading predation from C (Figures 5B and 5E). We conclude that when A inhibits B aggregation, this results in stronger predation of B by C, thus driving bacterial abundances down in time.

Taken together, the findings presented in Figures 2, 4, and 5 show that A reduces B aggregation, which renders the bacteria susceptible to predation by C. When the interaction between two species is modified by the presence of a third, this process is often termed ''higher order'' because all three species must be present in order for this interaction to affect the abundance dynamics of B. In order to confirm that such an interaction would explain our data and also to generalize our result, we sought a quantitative model of the dynamics in this community (Box 1).

Impact of Higher-Order Interaction Is Apparent in ABC Tri-culture Abundance Dynamics

We asked whether the model (Box 1; Equations 4, 5, 6, 7, and 8) could provide non-trivial predictions regarding community

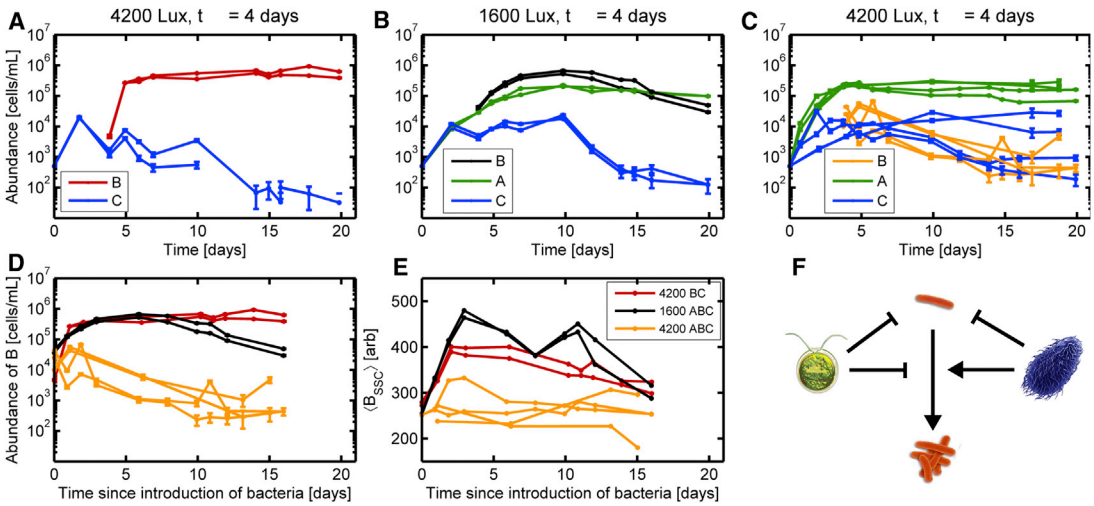

Figure 5. Algae Inhibit Bacterial Aggregation Enhancing Ciliate Predation, Resulting in Invasion Failure

(A–C) A and C abundances are shown in green and blue, respectively, in all panels. Color of B traces differs between (A)–(C) as shown in the legends. (A) Abundance dynamics for two replicates of a 4,200 Lux (high light) t_{inv} = 4 day B invasion on a C culture. (B) Abundance dynamics for two replicates of a 1,600 Lux (low light) t_{inv} = 4 day B invasion on an AC culture. A density is $2 \times 10^4 mL^{-1}$ at the time of B introduction. (C) Abundance dynamics for four replicates of a 4,200 Lux (high light) t_{inv} = 4 day B invasion on an AC culture. A density is $> 1 \times 10^5 mL^{-1}$ at the time of B introduction. Abundances are measured via flow cytometry. Error bars are computed as described in the STAR Methods. For time points where error bars are not visible, errors are smaller than the size of the points. B abundances are reported as the total number of cells including planktonic cells and cells in aggregates (see Figure S1).

(D) Overlay of B abundances from (A) (B), and (C), translated so that $t = 0$ corresponds to the time of B introduction.

(E) Overlay of mean side-scatter signal of (B) translated so that $t = 0$ corresponds to the time of B introduction. Colors of traces in (D) and (E) correspond to (A)–(C).

(F) Diagram of interactions between A, B, and C. Blunt arrowhead from C to planktonic B indicates C reducing B abundances. Blunt arrowhead from A to B indicates the inhibition of B growth by A. Arrows from A and C to the transition between planktonic and aggregated B indicate their respective impacts on B aggregation. (A), (B), and (C) are reproduced from Figures 2D, 2C, and 2F, respectively. For more data on how C enhances B aggregation, see Figure S4.

dynamics. We note that all parameters in the model are determined either from invasion data or from monoculture or pair-culture experiments. Therefore, to investigate, we simulated the dynamics of the ABC tri-culture under the two light regimes. The model predicts that under high light conditions, where x_A rapidly approaches K_A, bacterial abundances ($x_B + A_B$) are attenuated at long times. In contrast, for low light conditions where x_A does not reach high density until the very end of the experiment, our model predicts limited attenuation of bacterial abundances (compare Figures 6C and 6D). The lower bacterial abundances observed in our simulation at high light arise from reduced bacterial aggregation and increased predation of B by C (Figure 6F).

To test the predictions of the model, we performed tri-culture experiments with the full ABC community at low and high light levels. The dynamics are shown in Figures 6I and 6J. In the full ABC ecosystem, the growth rate of A differs by more than a factor of 4 between the two light levels ($0.016\ h^{-1}$ for low light versus $0.073 h^{-1}$ for high light). The slow growth rate of A in low light results in A reaching saturation only after 14 days. In contrast, in high light, A reaches saturating densities in 4 days. When we compare the dynamics of B in the full ABC ecosystem in low and high light, we observe that high light results in a substantial decline in bacterial abundances by the end of the experiment (Figure 6K, purple and black traces). In contrast, when B is grown with only C (and not A) in high light, there is no decline in B abundances at long times (Figure 6K, orange and purple traces). When we examine the bacterial aggregation state in the ABC low light and high light conditions, we find less B aggregation in the high light condition (Figure 6L). The results shown in Figure 6 do not depend on the aggregate correction algorithm we applied to bacterial abundances (Figure S3).

DISCUSSION

Our results show that phototrophs can indirectly decrease the population density of heterotrophic bacteria by modification of the nature of bacterial interactions with predators. Phototroph-heterotroph interactions are known to be mediated by competition and cross-feeding (Sher et al., 2011), but our data provide a new mode by which phototrophs might keep faster-growing heterotrophs from consuming available nutrients such as nitrogen or phosphorous.

In the context of the invasion literature, recently summarized by Mallon et al. (2015), our results show that resource competition alone is insufficient for predicting the outcome of invasions in communities where antagonistic interactions such as predation are present. The result has important implications for understanding community structure from coral reefs to wastewater treatment facilities where such interactions are known to be important (Ravva et al., 2013; Rodriguez-Brito et al., 2010).

We have shown that the ABC system exhibits what we term a higher-order interaction. Our usage of the term "higher order" is consistent with the ecological literature on the subject (Billick and Case, 1994) but deserves some clarification. What we have shown is that the collective impact of A and C on the aggregation of B results in a change in B abundances that is not observed in communities of A and B or B and C alone. The

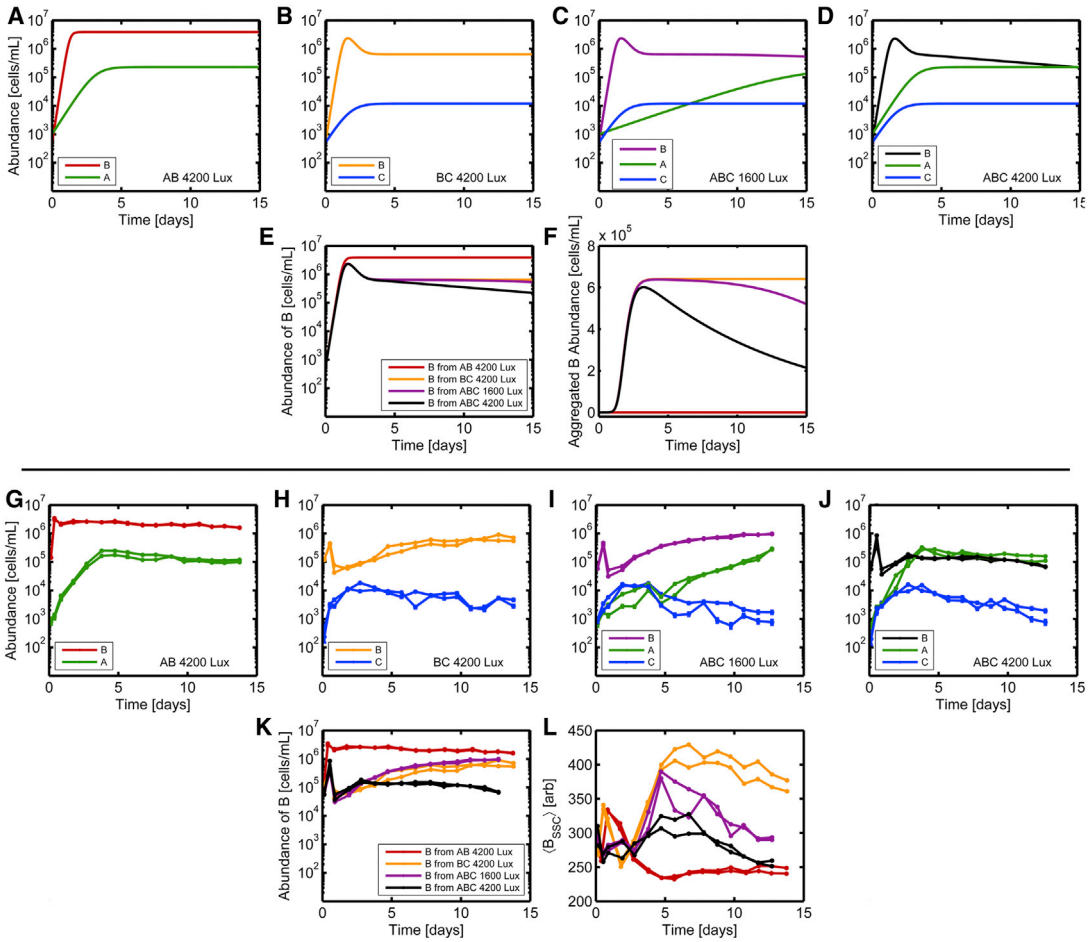

Figure 6. Higher-Order Interaction Impacts Algae-Bacteria-Ciliate Tri-culture Abundance Dynamics

(A–F) Simulations of abundance dynamics for the model given in Equations 4, 5, 6, 7, and 8 in tri-culture conditions where all species are introduced at low density at $t = 0$ days. All model parameters are given in Table S3. In all panels, x_A and x_C are shown in green and blue, respectively. The color of B ($x_B + A_B$) varies as indicated in (A)–(D) to facilitate the overlay plots in (E) and (F), which show total B abundances ($x_B + A_B$ (E)) and aggregating cell abundances (A_B only (F)). The legend from (E) applies to (F).

(G–L) Experimental measurements of tri-culture abundance dynamics corresponding to (A)–(F). Replicate communities are shown in each condition. Abundances are measured via flow cytometry. Error bars are computed as described in the STAR Methods. For time points where error bars are not visible, errors are smaller than the size of the points. B abundances are reported as the total number of cells including planktonic cells and cells in aggregates (see Figure S1). Note that the color of the traces for B abundances in (G)–(J) correspond to those in (A)–(D) as indicated in the legends. (J) Mean side scatter (which is a proxy for level of aggregation) of the B population from (G)–(J). The legend from (K) applies to (L). (K) Overlay of abundance dynamics for B from (G)–(J).

See also Figure S3 and Tables S2 and S3

impact of A and C on B is therefore what ecologists have termed an interaction modification (Wootton, 1994). Interaction modifications are higher order in the sense that they require a term that is the product of three species abundances when using a model that characterizes the impact of each species on the per capita growth rate of other species via effective interactions (Bairey et al., 2016; Billick and Case, 1994). However, a model that includes a more detailed specification of the bacterial population (planktonic and aggregated cells) does not require such a term. We have shown that a model that neglects the phenotypic differentiation in the bacterial population and subsumes these effects into effective interactions indeed contains a three-body term ($x_A x_B x_C$), as expected from theory. We therefore conclude that the process we observe is a higher-order interaction. We note that our usage of the term higher-order interaction is consistent with this ecological definition of higher-order processes but not with more stringent definitions in physics.

Recent theoretical studies exploring models that describe community dynamics at the level of abundances (e.g., Equation 1), but neglect microscopic details such as metabolites and phenotypes, suggest that higher-order interactions (interaction modifications) of the type studied here enhance the stability of complex communities. In contrast, communities where abundance dynamics can be described by pairwise interactions at the level of abundances become less stable as complexity increases (Bairey et al., 2016; Grilli et al., 2017). The results suggest that higher-order interactions may be important for explaining the complexity of natural communities.

Several studies have previously detected the presence of higher-order interactions (Losey and Denno, 1998; Wootton, 1994). For example, a recent study of interactions between *Streptomyces* soil isolates mediated by antibiotic excretions showed similar interaction modification effects (Abrudan et al., 2015). Moreover, statistical analyses of interactions between limpets, barnacles, and algae suggested the presence of a higher-order interaction whereby barnacles interfere with limpet grazing of algae (Dungan, 1986). However, direct measurements of the impact of higher-order interactions on invasions is limited. In contrast, several studies of dynamics in communities where interactions are mediated by resource competition have shown that pairwise interactions are sufficient to describe community dynamics (Friedman et al., 2017; Vandermeer, 1969). Our study shows that for a model community that includes predation and little or no competition for resources, higher-order interactions are not only present but also have substantial impacts on dynamics (Figure 6). To move theory closer to observation and experiment, it will be critical to investigate whether higher-order interactions are more common when predation is present or not.

Two previous studies on the ABC community, or a closely related ecosystem with *C. reinhardtii* replaced with *Euglena gracilis*, under hermetically sealed conditions have looked at interactions between these species. One study compared interactions inferred from abundance fluctuations in the full three species community to interactions measured via pair-culture experiments (Hekstra et al., 2013). A second study also used pairwise experiments (Matsui et al., 2000). In the case of the pairwise experiments, both studies detected evidence for the antagonistic effect of A and C on B. Interestingly, inference of pairwise interactions from abundance fluctuations in an ensemble of ABC communities did not identify these negative interactions (Hekstra et al., 2013) and instead inferred positive effects between all three species. This result points to the challenge of inferring interactions from fluctuations in time series data (Fisher and Mehta, 2014; Ives et al., 2003; Stein et al., 2013). Inferring interactions from fluctuations should work well near a fixed point of the community dynamics. However, understanding the full non-linear dynamics governing the community is likely a necessity for predicting the outcome of processes such as invasion where abundances can change by several orders of magnitude. Finally, neither previous study of the ABC system made a statement about the presence of higher-order effects in the community or the mechanisms mediating these interactions.

More broadly, our study has important implications for understanding the structure of natural microbial communities where primary production is driven by phototrophic microbes. In these ecological contexts, phototrophs exist not in isolation but in close association with heterotrophic bacteria (Stocker et al., 2008). Chemically mediated direct interactions between phototrophic algae, diatoms and cyanobacteria, and their associated heterotrophic bacterial communities are characterized by signaling interactions (Teplitski et al., 2004), competition, and antagonism (Paul and Pohnert, 2011). It has been observed that specific bacterial taxa often adhere directly to the surface of phototrophic microbes (Kimbrel et al., 2019), and this close physical proximity likely facilitates efficient exchange of metabolites. These interactions are thought to link the abundance dynamics of phototrophic microbes and their associated heterotrophic bacteria. For example, bacterial successions appear to be driven by carbon excreted by phototrophs during blooms (Teeling et al., 2012), and competition for nitrogen and phosphorous is believed to play a key role in phototroph-heterotroph interactions (Cole, 1982).

However, the role of phototrophs in mediating interactions between bacteria and their predators is not widely appreciated. The enhancement of predation pressure on bacteria due to the presence and metabolic activity of phototrophs might provide an indirect mechanism by which phototrophs can outcompete faster-growing heterotrophic bacteria for essential nutrients. For predators, our results suggest that phototrophs might unlock bacterial populations from aggregates, potentially driving associations between phototrophic microbes and protozoa. In the future, it will be important to connect these collective effects on population dynamics to the fluxes of nutrients such as carbon, nitrogen, and phosphorous through the community, which play a key role in the biogeochemical cycles on Earth.

STAR★METHODS

Detailed methods are provided in the online version of this paper and include the following:

- KEY RESOURCES TABLE
- LEAD CONTACT AND MATERIALS AVAILABILITY
- EXPERIMENTAL MODEL AND SUBJECT DETAILS
  - Strains
  - Culturing
  - Control of Initial Conditions
  - Experimental Conditions
- METHOD DETAILS
  - Sampling of Communities for Flow Cytometry
  - Abundance Measurement by Flow Cytometry
  - Calibration of Flow Rate to Infer Densities
  - Spent Media Experiments
  - Algae and Ciliate Growth Rates
  - Bacterial Aggregation
  - Culture Devices and Conditions
  - Construction of bacterial aggregate correction algorithm
  - Ciliates Cause Bacteria to Aggregate
  - Light Level Does Not Appear to Affect Bacterial or Ciliate Abundance Dynamics
  - Algae-Bacteria Interactions
  - Live-dead Staining Experiments
  - Successful Bacterial Invasions Are not an Artifact of Mis-classifying Algae Detritus as Bacteria
  - Modeling: Lotka-Volterra Model with Higher Order Interaction
  - Modeling: Details of Model Including Bacterial Aggregation
  - Bacteria-ciliate Interactions
  - Predation Rates and Functional Form
  - Algae-Bacteria Interactions
  - Aspects of the Dynamics Not Captured by the Model Including Bacterial Aggregation
  - Simulations
- QUANTIFICATION AND STATISTICAL ANALYSIS

SUPPLEMENTAL INFORMATION

Supplemental Information can be found online at https://doi.org/10.1016/j.cels.2019.11.004.

ACKNOWLEDGMENTS

The authors acknowledge Jason Merritt, Karna Gowda, Barbara Pilas, and Elizabeth Ujhelyi. Additionally, the authors acknowledge support from the Department of Physics, the Carl R. Woese Institute for Genomic Biology, and the Roy J. Carver Biotechnology Center, all at the University of Illinois at Urbana-Champaign. The authors thank Aaron Bell for permission to use the image of the ciliate. The authors also acknowledge support from the National Science Foundation Physics Frontier Centers Program (PHY 0822613 and PHY 1430124).

AUTHOR CONTRIBUTIONS

Conceptualization, H.M. and S.K.; Methodology, H.M. and S.K.; Investigation, H.M.; Writing, H.M. and S.K.

DECLARATION OF INTERESTS

The authors declare no competing interests.

Received: March 25, 2019
Revised: July 26, 2019
Accepted: November 7, 2019
Published: December 11, 2019

REFERENCES

Abrudan, M.I., Smakman, F., Grimbergen, A.J., Westhoff, S., Miller, E.L., van Wezel, G.P., and Rozen, D.E. (2015). Socially mediated induction and suppression of antibiosis during bacterial coexistence. Proc. Natl. Acad. Sci. USA *112*, 11054–11059.

Baba, T., Ara, T., Hasegawa, M., Takai, Y., Okumura, Y., Baba, M., Datsenko, K.A., Tomita, M., Wanner, B.L., and Mori, H. (2006). Construction of Escherichia coli K-12 in-frame, single-gene knockout mutants: the Keio collection. Mol. Syst. Biol. *2*, 2006.0008.

Bairey, E., Kelsic, E.D., and Kishony, R. (2016). High-order species interactions shape ecosystem diversity. Nat. Commun *7*, 12285.

Billick, I., and Case, T.J. (1994). Higher order interactions in ecological communities: what are they and how can they be detected? Ecology *75*, 1529–1543.

Blom, J.F., Zimmermann, Y.S., Ammann, T., and Pernthaler, J. (2010). Scent of danger: floc formation by a freshwater bacterium is induced by supernatants from a predator-prey coculture. Appl. Environ. Microbiol. *76*, 6156–6163.

Bovallius, A., Bucht, B., Roffey, R., and Anäs, P. (1978). Three-year investigation of the natural airborne bacterial flora at four localities in Sweden. Appl. Environ. Microbiol. *35*, 847–852.

Cassidy-Hanley, D., Smith, H.R., and Bruns, P.J. (1995). A simple, efficient technique for freezing Tetrahymena thermophila. J. Eukaryot. Microbiol. *42*, 510–515.

Chambouvet, A., Morin, P., Marie, D., and Guillou, L. (2008). Control of toxic marine dinoflagellate blooms by serial parasitic killers. Science *322*, 1254–1257.

Cole, J.J. (1982). Interactions between bacteria and algae in aquatic ecosystems. Ann Rev. Ecol. Syst *13*, 291–314.

Corno, G., and Jürgens, K. (2006). Direct and indirect effects of protist predation on population size structure of a bacterial strain with high phenotypic plasticity. Appl. Environ. Microbiol. *72*, 78–86.

Curds, C.R., and Cockburn, A. (1968). Studies on the growth and feeding of Tetrahymena pyriformis in axenic and monoxenic culture. J. Gen. Microbiol. *54*, 343–358.

Dawes, J.H., and Souza, M.O. (2013). A derivation of Holling's type I, II and III functional responses in predator-prey systems. J. Theor. Biol. *327*, 11–22.

Dungan, M.L. (1986). Three-way interactions: barnacles, limpets, and algae in a Sonoran Desert rocky intertidal zone. Am. Nat *127*, 292–316.

Elowitz, M.B., Levine, A.J., Siggia, E.D., and Swain, P.S. (2002). Stochastic gene expression in a single cell. Science *297*, 1183–1186.

Elton, C.S. (1958). The Ecology of Invasions by Animals and Plants, First Edition (Springer).

Fenchel, T. (1980a). Suspension feeding in ciliated protozoa: feeding rates and their ecological significance. Microb. Ecol *6*, 13–25.

Fenchel, T. (1980b). Suspension feeding in ciliated protozoa: functional response and particle size selection. Microb. Ecol *6*, 1–11.

Fierer, N., and Jackson, R.B. (2006). The diversity and biogeography of soil bacterial communities. Proc. Natl. Acad. Sci. USA *103*, 626–631.

Fisher, C.K., and Mehta, P. (2014). Identifying keystone species in the human gut microbiome from metagenomic timeseries using sparse linear regression. PLoS One *9*, e102451.

Frentz, Z., Kuehn, S., and Leibler, S. (2015). Strongly deterministic population dynamics in closed microbial communities. Phys. Rev. X *5*, 041014.

Friedman, J., Higgins, L.M., and Gore, J. (2017). Community structure follows simple assembly rules in microbial microcosms. Nat. Ecol. Evol. *1*, 0109.

Grilli, J., Barabás, G., Michalska-Smith, M.J., and Allesina, S. (2017). Higher-order interactions stabilize dynamics in competitive network models. Nature *548*, 210–213.

Hasman, H., Schembri, M.A., and Klemm, P. (2000). Antigen 43 and type 1 fimbriae determine colony morphology of *Escherichia coli* K-12. J. Bacteriol *182*, 1089–1095.

Hatzis, C., Srienc, F., and Fredrickson, A.G. (1994). Feeding heterogeneity in ciliate populations: effects of culture age and nutritional state. Biotechnol. Bioeng *43*, 371–380.

Hatzis, C., Sweeney, P.J., Srienc, F., and Fredrickson, A.G. (1993). Determination of cellular rate distributions in microbial cell populations: feeding rates of ciliated protozoa. Biotechnol. Bioeng *42*, 284–294.

Hekstra, D.R. (2009). Population Dynamics in a Model Closed Ecosystem (Rockefeller University).

Hekstra, D.R., Cocco, S., Monasson, R., and Leibler, S. (2013). Trend and fluctuations: analysis and design of population dynamics measurements in replicate ecosystems. Phys. Rev. E Stat. Nonlin. Soft Matter Phys. *88*, 062714.

Hekstra, D.R., and Leibler, S. (2012). Contingency and statistical laws in replicate microbial closed ecosystems. Cell *149*, 1164–1173.

Hillen, T., and Swan, A. (2016). The diffusion limit of transport equations in biology. In Mathematical Models and Methods for Living Systems. Lecture Notes in Mathematics, L. Preziosi, M. Chaplain, and A. Pugliese, eds. (Springer), pp. 73–129.

Hodgson, D.J., Rainey, P.B., and Buckling, A. (2002). Mechanisms linking diversity, productivity and invasibility in experimental bacterial communities. Proc. Biol. Sci. *269*, 2277–2283.

Hom, E.F., and Murray, A.W. (2014). Plant-fungal ecology. Niche engineering demonstrates a latent capacity for fungal-algal mutualism. Science *345*, 94–98.

Ishii, S., Ksoll, W.B., Hicks, R.E., and Sadowsky, M.J. (2006). Presence and growth of naturalized Escherichia coli in temperate soils from Lake Superior watersheds. Appl. Environ. Microbiol. *72*, 612–621.

Ito, A., May, T., Kawata, K., and Okabe, S. (2008). Significance of rpoS during maturation of Escherichia coli biofilms. Biotechnol. Bioeng *99*, 1462–1471.

Ives, A.R., Dennis, B., Cottingham, K.L., and Carpenter, S.R. (2003). Estimating community stability and ecological interactions from time-series data. Ecol. Monogr *73*, 301–330.

Jost, J.L., Drake, J.F., Fredrickson, A.G., and Tsuchiya, H.M. (1973). Interactions of Tetrahymena pyriformis, Escherichia coli, Azotobacter vinelandii, and glucose in a minimal medium. J. Bacteriol *113*, 834–840.

Junglee, S., Urban, L., Sallanon, H., and Lopez-Lauri, F. (2014). Optimized assay for hydrogen peroxide determination in plant tissue using potassium iodide. Am. J. Anal. Chem. *5*, 730–736.

Kawabata, Z., Matsui, K., Okazaki, K., Nasu, M., Nakano, N., and Sugai, T. (1995). Synthesis of a species-defined microcosm with protozoa. J. Protozool. Res. *5*, 23–26.

Kearns, K.D., and Hunter, M.D. (2000). Green algal extracellular products regulate antialgal toxin production in a cyanobacterium. Environ. Microbiol. *2*, 291–297.

Kimbrel, J.A., Samo, T.J., Ward, C., Nilson, D., Thelen, M.P., Siccardi, A., Zimba, P., Lane, T.W., and Mayali, X. (2019). Host selection and stochastic effects influence bacterial community assembly on the microalgal phycosphere. Algal Research *40*, 101489.

Kirchman, D.L. (2012). Processes in Microbial Ecology, First Edition (Oxford University Press).

Kjaergaard, K., Schembri, M.A., Hasman, H., and Klemm, P. (2000). Antigen 43 from Escherichia coli induces inter- and intraspecies cell aggregation and changes in colony morphology of Pseudomonas fluorescens. J. Bacteriol *182*, 4789–4796.

Laganenka, L., Colin, R., and Sourjik, V. (2016). Chemotaxis towards autoinducer 2 mediates autoaggregation in Escherichia coli. Nat. Commun *7*, 12984.

Letcher, P.M., Lopez, S., Schmieder, R., Lee, P.A., Behnke, C., Powell, M.J., and McBride, R.C. (2013). Characterization of Amoeboaphelidium protococcarum, an algal parasite new to the cryptomycota isolated from an outdoor algal pond used for the production of biofuel. PLoS One *8*, e56232.

Leupold, M., Hindersin, S., Gust, G., Kerner, M., and Hanelt, D. (2013). Influence of mixing and shear stress on Chlorella vulgaris, Scenedesmus obliquus, and Chlamydomonas reinhardtii. J. Appl. Phycol *25*, 485–495.

Losey, J.E., and Denno, R.F. (1998). Positive predator–predator interactions: enhanced predation rates and synergistic suppression of aphid populations. Ecology *79*, 2143–2152.

Lu, N., Sanchez-Gorostiaga, A., Tikhonov, M., and Sanchez, A. (2019). Cohesiveness in microbial community coalescence. bioRxiv. https://doi.org/10.1101/282723.

Mallon, C.A., Elsas, J.D.V., and Salles, J.F. (2015). Microbial invasions: the process, patterns, and mechanisms. Trends Microbiol. *23*, 719–729.

Matsui, K., Kono, S., Saeki, A., Ishii, N., Min, M.-G., and Kawabata, Zi (2000). Direct and indirect interactions for coexistence in a species-defined microcosm. Hydrobiologia *435*, 109–116.

Merritt, J., and Kuehn, S. (2016). Quantitative high-throughput population dynamics in continuous-culture by automated microscopy. Sci. Rep *6*, 33173.

Merritt, J., and Kuehn, S. (2018). Frequency- and amplitude-dependent microbial population dynamics during cycles of feast and famine. Phys. Rev. Lett. *121*, 098101.

Morris, J.J., Johnson, Z.I., Szul, M.J., Keller, M., and Zinser, E.R. (2011). Dependence of the cyanobacterium Prochlorococcus on hydrogen peroxide scavenging microbes for growth at the ocean's surface. PLoS One *6*, e16805.

Olsén, A., Jonsson, A., and Normark, S. (1989). Fibronectin binding mediated by a novel class of surface organelles on Escherichia coli. Nature *338*, 652–655.

Paul, C., and Pohnert, G. (2011). Interactions of the algicidal bacterium Kordia algicida with diatoms: regulated protease excretion for specific algal lysis. PLoS One *6*, e21032.

Pouneva, I. (1997). Evaluation of algal culture viability and physiological state by fluorescent microscopic methods. Bulg. J. Plant Physiol *23*, 67–76.

Ravva, S.V., Sarreal, C.Z., and Mandrell, R.E. (2013). Altered protozoan and bacterial communities and survival of Escherichia coli O157:H7 in monensin-treated wastewater from a dairy lagoon. PLoS One *8*, e54782.

Roach, T., Na, C.S., and Krieger-Liszkay, A. (2015). High light-induced hydrogen peroxide production in Chlamydomonas reinhardtii is increased by high CO_2 availability. Plant J *81*, 759–766.

Rodriguez-Brito, B., Li, L., Wegley, L., Furlan, M., Angly, F., Breitbart, M., Buchanan, J., Desnues, C., Dinsdale, E., Edwards, R., et al. (2010). Viral and microbial community dynamics in four aquatic environments. ISME J *4*, 739–751.

Sack, L., Zeyl, C., Bell, G., Sharbel, T., Reboud, X., Bernhardt, T., and Koelewyn, H. (1994). Note. Isolation of four new strains of Chlamydomonas-reinhardtii (Chlorophyta) from soil samples. J. Phycol *30*, 770–773.

Seto, M., and Tazaki, T. (1971). Carbon dynamics in the food chain system of glucose-Escherichia coli-Tetrahymena vorax. Jpn. J. Ecol *21*, 179–188.

Seymour, J.R., Amin, S.A., Raina, J.B., and Stocker, R. (2017). Zooming in on the phycosphere: the ecological interface for phytoplankton-bacteria relationships. Nat. Microbiol. *2*, 17065.

Sher, D., Thompson, J.W., Kashtan, N., Croal, L., and Chisholm, S.W. (2011). Response of Prochlorococcus ecotypes to co-culture with diverse marine bacteria. ISME J *5*, 1125–1132.

Shimoyama, T., Kato, S., Ishii, S., and Watanabe, K. (2009). Flagellum mediates symbiosis. Science *323*, 1574.

Stein, R.R., Bucci, V., Toussaint, N.C., Buffie, C.G., Rätsch, G., Pamer, E.G., Sander, C., and Xavier, J.B. (2013). Ecological modeling from time-series inference: insight into dynamics and stability of intestinal microbiota. PLoS Comput. Biol. *9*, e1003388.

Stocker, R., Seymour, J.R., Samadani, A., Hunt, D.E., and Polz, M.F. (2008). Rapid chemotactic response enables marine bacteria to exploit ephemeral microscale nutrient patches. Proc. Natl. Acad. Sci. USA *105*, 4209–4214.

Taub, F.B., and Dollar, A.M. (1964). A chlorella-daphnia food-chain study: the design of a compatible chemically defined culture medium. Limnol. Oceanogr *9*, 61–74.

Taub, F.B., and Dollar, A.M. (1968). The nutritional inadequacy of Chlorella and Chlamydomonas as food for Daphnia pulex. Limnol. Oceanogr *13*, 607–617.

Teeling, H., Fuchs, B.M., Becher, D., Klockow, C., Gardebrecht, A., Bennke, C.M., Kassabgy, M., Huang, S., Mann, A.J., Waldmann, J., et al. (2012). Substrate-controlled succession of marine bacterioplankton populations induced by a phytoplankton bloom. Science *336*, 608–611.

Teplitski, M., Chen, H., Rajamani, S., Gao, M., Merighi, M., Sayre, R.T., Robinson, J.B., Rolfe, B.G., and Bauer, W.D. (2004). Chlamydomonas reinhardtii secretes compounds that mimic bacterial signals and interfere with quorum sensing regulation in bacteria. Plant Physiol. *134*, 137–146.

Tikhonov, M. (2016). Community-level cohesion without cooperation. Elife *5*, e15747.

Tilman, D. (1997). Community invasibility, recruitment limitation, and grassland biodiversity. Ecology *78*, 81–92.

van Elsas, J.D., Chiurazzi, M., Mallon, C.A., Elhottova, D., Kristufek, V., and Salles, J.F. (2012). Microbial diversity determines the invasion of soil by a bacterial pathogen. Proc. Natl. Acad. Sci. USA *109*, 1159–1164.

Vandermeer, J.H. (1969). The competitive structure of communities: an experimental approach with protozoa. Ecology *50*, 362–371.

Vetsigian, K., Jajoo, R., and Kishony, R. (2011). Structure and evolution of Streptomyces interaction networks in soil and in silico. PLoS Biol. *9*, e1001184.

Wei, Z., Yang, T., Friman, V.P., Xu, Y., Shen, Q., and Jousset, A. (2015). Trophic network architecture of root-associated bacterial communities determines pathogen invasion and plant health. Nat. Commun *6*, 8413.

Widder, S., Allen, R.J., Pfeiffer, T., Curtis, T.P., Wiuf, C., Sloan, W.T., Cordero, O.X., Brown, S.P., Momeni, B., Shou, W., et al. (2016). Challenges in microbial ecology: building predictive understanding of community function and dynamics. ISME J *10*, 2557–2568.

Wojtaszek, P. (1997). Oxidative burst: an early plant response to pathogen infection. Biochem. J. *322*, 681–692.

Wootton, J.T. (1994). The nature and consequences of indirect effects in ecological communities. Annu. Rev. Ecol. Syst. *25*, 443–466.

STAR★METHODS

KEY RESOURCES TABLE

REAGENT or RESOURCE	SOURCE	IDENTIFIER
Bacterial and Virus Strains		
Escherichia coli ns2. ΔfimA Δflu	Hekstra and Leibler. *Cell* 2012.	N/A
Escherichia coli. intC::YFP	Wang *et al. Curr. Biol.* 2010	SJ102
Escherichia coli . ΔcsgA	Coli Genetic Stock Center	8997
Phage P1	N/A	N/A
Deposited Data		
Raw abundance measurements by flow cytometry and code for simulations.	This work	https://doi.org/10.13012/B2IDB-0946028_V1
Experimental Models: Organisms/Strains		
Chlamydomonas reinhardtii UTEX 2244 (cc-125 WT mt+)	University of Texas culture collection of algae	2244
Tetrahymena thermophile CU428.2 (*mpr1-1/mpr1-1* (*MPR1*; mp-s, VII))	Cornell University Tetrahymena Stock Center	TSC_SD00178

LEAD CONTACT AND MATERIALS AVAILABILITY

Further information and requests for resources and reagents should be directed to and will be fulfilled by the Lead Contact, Seppe Kuehn (seppe.kuehn@gmail.com). The study did not generate new materials. Flow cytometry data and code for simulations are freely available, see Key Resources Table.

EXPERIMENTAL MODEL AND SUBJECT DETAILS

Strains

The alga is *C. reinhardtii*, strain UTEX2244 obtained from the University of Texas Austin Culture Collection of Algae utex.org. All *C. reinhardtii* cells are of a single mating type mt+ and grow vegetatively. Algae are cryogenically preserved and stored in liquid nitrogen https://utex.org/pages/cryopreservation#liquid. The *E.coli* strain is MG1655 Δ*flu*, Δ*fimA* and was constructed previously (Hekstra and Leibler, 2012). These mutations reduce biofilm formation and aggregation, *flu* encodes a cell-cell adhesion protein (*Ag43*) and *fimA* a structural unit of fimbrae (Hasman et al., 2000; Kjaergaard et al., 2000). A constitutively expressed yellow fluorescent protein (YFP, promoter λP_R) was transduced into the genome with phage P1. The donor strain for YFP fluorescence has the YFP gene inserted in the *intC* locus along with a chloramphenicol antibiotic resistance marker (Elowitz et al., 2002). The Δ*csgA* strain was constructed by P1 transduction from KEIO collection (Baba et al., 2006) mutant into MG1655 (WT) background. The same YFP construct was also transduced into this strain. The ciliate is *T. thermophila*, strain CU428.2 obtained from the Cornell University Tetrahymena Stock Center https://tetrahymena.vet.cornell.edu/. All *T. thermophila* cells are of mating type VII so there is only asexual reproduction. This strain grows vegetatively indefinitely without sexual reproduction. Ciliates were cryogenically frozen and stored in liquid nitrogen (Cassidy-Hanley et al., 1995).

Culturing

Before beginning the experiment, each of the organisms is cultured separately in distinct media. A is cultured in a 30°C shaker-incubator with ~3000 Lux illumination in Tris-Acetate-Phosphate (TAP) media inoculated directly from a freezer stock. Algae used in co-culture experiments (low-light), A, AC, ABC and (high light) A, AC and ABC were grown at 25°C prior to the experiment. TAP is a defined media with acetic acid as a carbon source https://www.chlamycollection.org/methods/media-recipes/tap-and-tris-minimal/. C is cultured in a 30°C stationary incubator in (undefined) SPP media inoculated directly from a freezer stock. B was cultured in a 30 °C shaker-incubator in 1/2x Taub 0.03% proteose peptone No. 3 inoculated from a single colony grown on an lysogeny broth (LB) plate.

Control of Initial Conditions

The cultures of each of the three organisms are washed twice into 1/2x Taub .01% Proteose Peptone No. 3. Flow cytometry is performed on a sample from each washed culture to estimate cell densities. The cultures are then diluted into 1/2x Taub .01% proteose peptone No. 3 in order to achieve nominal densities of 500 ± 22 mL^{-1} for A, 1000 ± 32 mL^{-1} for B, and 500 ± 22 mL^{-1} for C. Error bars are assumed from Poisson counting error. Organisms are always started at these densities at the beginning of an experiment,

regardless of whether that experiment is monoculture, pair-culture, or tri-culture. For B invasion experiments the starting density was $\sim 1 \times 10^4 mL^{-1}$.

Experimental Conditions

All experiments are performed in 1/2x Taub .01% proteose peptone No. 3. This media is used because it is similar to media used in previous studies with the ABC community (Frentz et al., 2015; Hekstra and Leibler, 2012) and because each of the three organisms can grow on this media in monoculture, pair-culture, and tri-culture. Taub media is a freshwater mimic media that was originally created to support co-cultures of *Daphnia pulex* and *Chlorella pyrenoidosa* (Taub and Dollar, 1964; Hekstra, 2009). It contains 15μM H_3BO_3; 0.5μM $ZnSO_4$; 3.5μM $MnCl_2$; 0.5μM Na_2MoO_4; 0.1μM $CuSO_4$; 0.5μM $Co(NO_3)_2$; 100μM $MgSO_4$; 100μM KH_2PO_4; 5.6μM EDTA; 5.6μM $FeSO_4$; 1.5mM NaCl; and 1mM $CaCl_2$. Proteose peptone No. 3 is an undefined nutrient source that is an enzymatic digest of protein and supplies nitrogen and carbon [http://www.bdbiosciences.com/ds/ab/others/Proteose_Peptone_No_2_3_4.pdf]. The media is titrated to pH 7 before use.

Each of the eight vials are kept in an experimental apparatus for the duration of the experiment. The vial fits snugly into a metal block that is held at 30˚C via proportional-integral-derivative (PID) control. Temperature is measured by a thermometer embedded in the metal block and heating/cooling is performed by a Peltier element (Merritt and Kuehn, 2016). The temperature within a vial fluctuates with standard deviation 0.02˚C as determined by the feedback thermometer embedded in the metal block housing the vial. The temperature across the eight vials varies with standard deviation 0.08˚C as measured in a control experiment where each vial is filled with water and the temperature is measured using a high-accuracy Fisher Scientific Traceable Thermometer (p/n: 15-081-102) and taking the standard deviation across vials.

The vial is illuminated by a single LED (Cree XLamp XP-E2 Single 1 Up Neutral White 4000 K color temperature, LED Supply p/n: CREEXPE2-740-1) from below. The spectrum of the LEDs used in this study is shown in Figure S7. We report both lux (which is a measure of intensity spectrally weighted towards the green) and $\mu mol\, m^{-2}\, s^{-1}$ for those readers more familiar with the latter measure. To approximately convert between these two measures we used a conversion factor based on a Phillips Luxeon 4000 K color temperature LED (https://docs.agi32.com/AGi32/Content/adding_calculation_points/PPFD_Concepts.htm). The LED is driven by an LED driver (BuckPuck DC LED Driver LED Supply p/n: 03021-D-E-350) and the intensity of these LEDs was found to be too high for bacterial growth and is decreased through the use of a neutral density filter. The illuminance is further modulated by applying a voltage to the control pin of the LED Driver. Experiments are performed at either low light (1600 ± 140 Lux) or high light (4200 ± 330 Lux). These values represent the time-averaged illuminance an organism would experience assuming it spends an equal amount of time at each height in the vial. These values are calculated based on measurements of illuminance taken from the top of the metal block with a light meter (LED Light Meter p/n: PCE-LED 20). Error bars are standard deviation across systems. The light levels are on the same order of magnitude as those used in a previous study of the ABC ecosystem (Frentz et al., 2015). The experimental apparatus is mounted on a stir-plate (Thermo Scientific Cimarec-i Mono Direct Stirrer 50095601) that keeps cultures stirred at 444 ± 4 RPM. This rotation speed was measured with a custom Hall Probe. At this stirring rate in our vials the Reynolds number is 10^4 which is high enough to ensure homogenous mixing of the community. Mixing ensures that samples used for flow cytometry accurately represent abundances in the vial. At these stirring rates we expect shear stress to change algal photosynthetic activity by <5% (Leupold et al., 2013).

METHOD DETAILS

Sampling of Communities for Flow Cytometry

Samples of communities are taken via a syringe attached to a sterile port. 500μL are drawn from the vial for each sample. This process constitutes destructive sampling of the community. Over the course of a typical experiment, 16 samples are taken from the vial which corresponds to 8 mL being removed from the vial. The depth of liquid in the vial decreases by 1.65 cm from its initial depth of 6.25 cm.

Abundance Measurement by Flow Cytometry

Flow cytometry is performed using a Becton-Dickson LSR II. To count bacteria, YFP fluorescence is plotted versus side-scatter (SSC) and cells are gated manually. To count algae, Chlorophyll-b fluorescence is plotted versus YFP fluorescence and gated manually. To count ciliates, CFP fluorescence is plotted versus SSC and the gate is drawn manually. Correct gating is confirmed by making measurements on monocultures. Because of the size difference between bacteria and ciliates, the two organisms scatter vastly different amounts of light and so a different gain is appropriate for the SSC channel for each. We therefore run every flow sample on two different gain settings.

Calibration of Flow Rate to Infer Densities

To report densities we calibrate the liquid flow rate through the flow cytometer using Spherotech Accucount fluorescent beads (ACFP-50-5, 5.0-5.9 μm) which come at a known concentration of $2 \times 10^6 mL^{-1}$. The beads are diluted tenfold and run for 30 s, the same duration that ecosystem samples are run. From the number of beads detected in 30 s we compute a flow rate. For every

time point in the abundance data, we perform three replicates of this volume calibration. We assume that the volume calibration applies to all samples run at that time point (within ~1 hour of the calibration of the cytometer). Over the course of this study (2 years) we observed a decrease in the LSR II flow rate by 60%.

Spent Media Experiments

In spent media experiments, cultures are prepared and grown as normal. To obtain spent media, several hundred microliters are extracted from the culture and filtered through a 0.22 μm polyethersulfone (PES) filter. Spent media is stored at 4˚C until all spent media extractions are complete. Spent media is then added to a 96-well microtiter plate and inoculated with bacteria and, depending on the experiment, ciliates. The plate is shaken and incubated at 30˚C for two or three days so that bacteria can grow to saturation. Bacterial abundances are then measured via flow cytometry.

Algae and Ciliate Growth Rates

We calculated growth rates for algae and ciliates in all coculture experiments (Table S1). Growth rate was calculated by fitting a line to the linear portion of the natural logarithm of that species' abundance in time. Error on growth rate is calculated as a 95 % confidence interval. Algae growth rates at 1600 Lux (low light) were significantly different for different species compositions and we thus report a mean growth rate over replicates for each species composition. For algae at 4200 Lux (high light), or ciliates at either light level, growth rates were not significantly different across species compositions and we thus report a single mean growth rate over all replicates of all species compositions. Error on mean growth rate is calculated as standard deviation across replicates. We do not report growth rates here for bacteria since the time resolution of our flow cytometry measurement is too coarse to reliably measure bacterial growth rates. Bacterial growth rate is instead measured using continuous absorbance measurements in a plate reader.

Bacterial Aggregation

In the main text we report that side scatter signal of bacteria (YFP fluorescence) reflects the aggregation of bacteria, with higher side scatter levels indicating larger bacterial aggregates. Here we support this claim experimentally.

Vortex experiment confirms side-scatter measures aggregation High side-scatter bacterial objects were originally suspected to be aggregates of bacteria for two reasons. 1) Side-scatter is a measure of how much light is scattered at a 90 degree angle when an object passes through the flow cytometer and larger objects tend to scatter more light. Indeed the ciliates, the largest of the three organisms, has the highest side-scatter signal. Since aggregates of bacteria are larger than single cells, they should have higher side-scatter signal. 2) The high side-scatter portion of the bacterial population stays present throughout an experiment only when ciliates are present and ciliates are known to induce bacteria to aggregate (see main text for Discussion).

Culture Devices and Conditions

During the experiment, 30 mL of culture are grown in a glass vial (Chemglass CG-4902-08 40 mL volume). A 0.1 μm filter allows gas exchange between the culture and the atmosphere. We expect this gas exchange (venting) coupled with stirring allows the community to be rapidly equilibrated with atmospheric O_2 and CO_2 concentrations. Eight vials are run in parallel.

We performed a vortexing experiment to test if high side-scatter signal bacterial objects were indeed aggregates. In the experiment we performed flow cytometry on a sample of bacteria (Figure S1A), vortexed the sample, and then performed flow cytometry again (Figure S1B). We hypothesized that vortexing would break up aggregates. This hypothesis lead to two clear predictions: (1) that the number of bacterial objects would increase, due to aggregates being broken up into multiple objects, and (2) that vortexing would reduce the number of high side-scatter objects. Both predictions were confirmed. By comparing the bacterial object abundances from before and after vortexing, one can see that abundances increased after vortexing. By comparing the histograms of side scatter signal of bacterial objects (Figure S1C), one can see that the number of high side-scatter bacterial objects decreased after vortexing. In addition, one can see that vortexing does not affect the location of the peak of the histogram, which therefore presumably corresponds to single-celled bacteria and which are not disrupted by vortexing.

Construction of bacterial aggregate correction algorithm

In order to estimate the true number of bacterial cells, we devised a technique to estimate the number of bacterial cells in an aggregate. Having confirmed in the previous section that side-scatter signal correlates with the number of bacteria in an aggregate, we seek an expression for the number of bacteria (N) as a function of the magnitude of the side scatter signal for each object (S). We assume that for objects below a threshold value of $S<t$ then $N(S) = 1$. We set t to a value which corresponds to the right shoulder of the left mode of the distribution in Figure S1E. For aggregates, objects with $S>t$, we take the ansatz that $N(S) = \alpha S^{\beta}$

β is an exponent which represents how the number of cells in an aggregate scales with the side-scatter signal and α is a prefactor. We chose this form because it is monotonic with S, it is possible to infer these parameters from our data, and scattering theory for simple objects (e.g. spheres) shows that the scaling of scattered light intensity is polynomial in particle size.

The first step in determining α and β is to define t. t should be the value of side-scatter past which bacterial objects are predominantly aggregates. We estimate this value by plotting a histogram of side-scatter signal of bacteria and marking the point at which the approximately Gaussian curve (representing single cells) turns into a tail (Figure S1E). Based on visual inspection of histograms of side-scatter, we set $t = 300$.

In all flow cytometry data reported up to this point, what is reported is the *log* of the fluorescence or scattered intensity. When data files of the format used in this study (fcs2.0) are exported from the flow cytometer, all fluorescence/scattering intensities are given as integers on a scale from 0 to 1023 (10-bit ADC), where 0 represents no signal and 1023 represents a signal which saturates the photomultiplier tube. The user is given the option of whether they want the data to be log-transformed or not. Our data are log-transformed since this affords us a larger dynamic range. Therefore, our flow data report *log*(*S*) rather than S. In order to follow our ansatz above it is necessary to transform our flow cytometry data from a logarithmic to a linear scale. However, the coefficients of the exponential transformation are not given by the manufacturer of the instrument, so it was necessary to infer the parameters of this transformation. To accomplish this we exported a single dataset on a linear and log scale (e.g. *S* and *log*(*S*)). From these two datasets we inferred that:

$$S = 0.0899e^{.0092log(S)}$$

(Figure S1F) Therefore, our threshold on $log(S)$ of 300 is 1.41 on a linear scale.

We next inferred α and β from the vortexing experiment shown in Figures S1A–S1C. The key insight is that the *total* number of bacterial cells cannot change due to vortexing (although the number of detected objects does change due to vortexing disrupting aggregates). We employed the following method to determine α and β.

For a given run of the flow cytometer consider the *M* objects which are detected and classified as bacteria to be indexed by *i*. The side scatter signal from the *i*th object is then S_i which contains a number of bacterial cells $N(S_i)$. For sample *k* we denote the side scatter signals from all *M* objects prior to vortexing as $S_{i,p,k}$. For the same sample we refer to the side scatter for all objects *after* vortexing as $S_{i,v,k}$ where *i* now runs to *M′* with *M*<*M′*. For example, the distribution of $log(S_{i,p,k})$ is given by the purple traces in Figure S1C and the distribution of $log(S_{i,v,k})$ by the yellow traces.

Under the assumption that the number of cells (not objects) cannot change due to vortexing the following equality must hold:

$$\sum_{i}^{M} N(S_{i,p,k}) = \sum_{i}^{M'} N(S_{i,v,k})$$

from this we find that:

$$q = \frac{\sum_{i}^{M'} \alpha(S_{i,p,k})^{\beta}}{\sum_{i}^{M'} \alpha(S_{i,v,k})^{\beta}} = 1$$

Our objective then is to determine the values for α and β such that $q = 1$. We now consider $q(\alpha,\beta,k)$ which shows how the ratio of the number of inferred bacterial cells depends on α and β. A heatmap of $q(\alpha,\beta,1)$ is shown in Figure S1G with the important modification that we plot $1/q$ for values of $q < 1$. Local minima in this heatmap near 1 reveal values of α and β where our assumptions are satisfied. Note how the pairs of α and β along the ascending diagonal of this heatmap have $q \approx 1$. We now compute the same heatmap for $k = [1,2,3,4]$ and compute

$$\sum_{k=1}^{4} q(\alpha,\beta,k)^2$$

again taking $1/q$ when $q < 1$ (Figure S1H). This plot reveals a range of both α and β for which this sum is 4 where our assumptions are satisfied for all four samples in our vortex experiment. We applied the square to each element in the sum to especially penalize samples which had high q at the given α and β.

To narrow the range of parameters we apply a final criterion. Given our assumption that the lower mode of the distribution of *S* comes from single cells, we know that $N(S<1.41) \approx 1$. Therefore we computed $N(S = 1.41)$ as a function of α and β and the result is shown in Figure S1I. These criteria alone do not uniquely determine α and β so we proceed by selecting $\alpha = 0.9$ and $\beta = 0.7$ where $N(S = 1.41) = 1.14$. This decision is subjective, but does not dramatically alter our results. For all bacterial abundances reported in the main text we use this aggregate correction algorithm.

The success of the aggregation correction algorithm can be seen in how it eliminates a spurious drop in bacterial abundances that was caused by aggregation. In Figure S1J, we have plotted an abundance curve for bacteria in a 1600 Lux (low light) monoculture before and after the aggregate correction algorithm is applied. Before correction, all bacterial objects are weighted equally, meaning that an aggregate and a single cell are both counted as a single bacterium. This equal weighting leads to a spurious fall in bacterial abundance after reaching the initial peak. Notice how the apparent decline in bacterial abundance at day 1 corresponds in time to an increased level of aggregation (Figure S1K). Once the bacteria eventually disaggregate, around day 5 or so, the curve returns to its peak value. These apparent changes in bacterial density are due to aggregation and disaggregation, not an actual change in bacterial cell concentration. Our aggregate correction formula successfully eliminates these spurious abundance changes.

The primary results of this work do not depend on the application of the aggregate correction algorithm. More specifically, invasion outcomes and abundance dynamics in Figures 2 and 6 from the main text do not change qualitatively after application of the aggregate correction algorithm (Figures S2 and S3). The only case in which there is qualitative disagreement between aggregate-corrected B abundance and not-aggregate-corrected B abundance is the 1600 Lux (low light) t_{inv} = 4-d invasion of bacteria on AC as depicted in (C) of Figure 2. In the aggregate-corrected case, Figures 2C and 2B invades and rises to an abundance of $\sim 7 \times 10^5 mL^{-1}$. In contrast, in the not-aggregate-corrected case, B does not rise significantly above its abundance at introduction

and only reaches $\sim 1 \times 10^5 mL^{-1}$ (Figure S2C). The two possible explanations for this disagreement are (1) the B in this condition are highly aggregated and the aggregate correction algorithm has successfully estimated the true B abundance or (2) high SSC detritus from A and/or C has bled into the flow cytometry gate used to count B and has erroneously inflated the measure of B abundance by $\sim 6 \times 10^5 mL^{-1}$.

In order to test explanation (2), we applied the flow cytometry gate used to count B to 1600 Lux (low light) AC coculture data. At almost all timepoints in this data, no detritus fell within this gate. In just two cases did any AC detritus bleed into this gate and at most, $3 \times 10^3 mL^{-1}$ B abundance (aggregate-corrected) was erroneously measured. This value is two orders of magnitude smaller than necessary to explain the mismatch between B abundances when aggregate corrected (Figure 2C) and not aggregate-corrected (Figure S2) and so we therefore conclude that the successful invasion depicted in Figure 2C is real.

Ciliates Cause Bacteria to Aggregate

When bacteria from a 1600 Lux (low light) B monoculture (Figure S4A) are compared to bacteria from a 1600 Lux B invasion of C (Figure S4B), histograms of the side-scatter signal of bacteria show increased aggregation in the presence of the ciliates (Figure S4G). Note that both histograms have a peak at low side scatter signal which corresponds to planktonic bacterial cells.

Ciliate induces aggregation in a ΔcsgA E. coli mutant We attempted to test our statement more directly that ciliates prey on planktonic bacteria using mutants. We constructed a Δ*csgA* strain of *E. coli* (in an MG1655 background) that exhibited dramatically reduced aggregation in liquid culture (Figure S11, (Laganenka et al. 2016)). *csgA* encodes a structural subunit of the curli fimbrae which mediate cell-cell adhesion at temperatures below 37˚C (our experiments were all undertaken at 30˚C) (Olsén et al. 1989). As expected, monocultures of this mutant aggregate much less than monocultures of the strain used in all other experiments (Δ*flu*Δ*fimA*) (Figure S4L). Because of its lack of aggregation, we hypothesized that this non-aggregating mutant would be unable to invade a culture of ciliates. Surprisingly, we found that not only did the Δ*csgA* bacteria invade the ciliates (Figure S4K), but they also showed enhanced aggregation in the presence of C as compared to monoculture (Figures S4L and S4M yellow traces).

Light Level Does Not Appear to Affect Bacterial or Ciliate Abundance Dynamics

Experiments throughout the paper are performed at 1600 Lux (low light) and 4200 Lux (high light). We claim that the abundance dynamics of B and C are not impacted by illumination at either level of illumination. When comparing bacterial abundance dynamics between low light and high light conditions for the co-culture experiments, B behaves identically across light levels regardless of the species composition: B monoculture, AB co-culture, or BC co-culture (Figure S5). The only species composition in which B behaves differently across light levels is the ABC co-culture (Figures 6I and 6J). We argue in the main text that this effect is due to a higher-order interaction in the community. Second, we examined the growth rates of C in low and high light conditions. We pooled together the C growth rates in all communities (e.g. BC, AC, ABC) at the two light levels and performed a weighted linear regression on the categorical variable of light level (low/high). We weighted each measured growth rate in the regression with 1/Error from Table S1. We were unable to reject the null hypothesis that the average growth rate at high light is the same as at low light (constant model, $p = 0.12$). We conclude that there is no evidence of a strong phototoxic or inhibitory effect on the bacteria or the ciliates at these light levels.

We note that there is substantial variability in the C abundance dynamics. We believe that these differences reflect differences in the state of the ciliate population prior to starting the experiment (e.g. small variations in the growth phase at the time the experiment was initiated) since ciliate abundance dynamics are observed to be very similar between replicate populations started from the same culture (Figure S6).

Algae-Bacteria Interactions

When Algae Are at Sufficiently High Density, They Stochastically Prevent Bacterial Invasion

We performed a set of invasion experiments where B was introduced to A at $t = 0$ days (co-culture), 1 day, 3 days and 4 days all in high light (4200Lux) conditions. We found that A did not suppress B when A was at densities below $1 \times 10^5 mL^{-1}$ at time of bacterial introduction (Figures S8A and S8B), but that suppression did occur when B was introduced to high density A (Figures S8C and S8D). Of those six high-density A cultures which suppressed bacterial invasion, three completely prevented bacterial invasion (low bacterial densities of $\sim 1 \times 10^3 mL^{-1}$ even after two weeks), while the other three high-density A cultures allowed bacteria to grow to high density over the period of approximately two weeks following bacterial introduction.

Algae must be physically present and illuminated to inhibit bacterial invasion We performed an experiment to test the importance of the physical presence of algae in the suppression of bacterial invasions. A culture of algae was grown in a 1 L Erlenmeyer flask for ten days in a shaker incubator at approximately 4000 Lux, 30˚C, and 175 RPM. The algae culture was then transferred to vials and inoculated with bacteria at a density of $1 \times 10^5 mL^{-1}$. These vials were placed in the culture devices used for the experiments shown in the main text. In two replicates the brightness was set to 4200 Lux (high light) (Figure S8E) while in the other two replicates the brightness was set to 0 Lux (no light) (Figure S8F). Bacteria and algae abundance were then measured by flow cytometry.

In the other half of the experiment, the algae culture was filtered through a 0.22μm PES membrane filter before being distributed across vials and inoculating bacteria. Once again the vials were set to 4200 Lux (Figure S8G) and 0 Lux (Figure S8H).

The only condition in which bacterial invasion was inhibited was the condition with lights on and algae physically present (Figure S8E). In all other cases: lights-off, algae filtered out, or both, bacteria invaded immediately. The necessity of light implies that algae's photosynthetic metabolism must be active to suppress bacterial invasion.

The mechanism by which the physical presence of algae is necessary to inhibit invasion remains unclear. However, we present a few possible interpretations of this result: (1) Algae suppresses bacterial invasion by secreting a toxic compound, one that they only begin producing when they sense the presence of bacteria (microbes can be stimulated to emit toxins by presence of other microbes (Kearns and Hunter, 2000)) (2) Algae suppresses bacterial invasion by secreting a toxic compound which can be degraded by bacteria. In this scenario the toxin in the spent algal medium is rapidly degraded by the bacteria, but in the case where algae are present the production rate of the toxin exceeds the bacterial degradation rate of that toxin. This possibility motivated us to test H_2O_2 as the mechanism since algae produce reactive oxygen species and bacteria degrade them via catalase. Our experiments showed that hydrogen peroxide is not the mechanism of inhibition (see discussion below). (3) Physical contact between algae and bacteria is necessary for the mechanism of invasion suppression (flagella have been seen to mediate interactions between microbes (Shimoyama et al., 2009)). (4) Algae suppresses bacterial invasion by secreting a toxic compound that is larger than the pores of the 0.22μm filter.

Additional spent media experiments further support the claim that algae must be physically present to enhance ciliate predation of bacteria. To show this, two replicates of a 1600 Lux (low light) A monoculture were grown in the temperature/light-control systems. Samples were harvested at multiple time points and all algae cells were removed by filtration. B along with C was then inoculated into this spent media (Figure S9A) and grown to saturation in a 96-well plate where B's density K_B was assayed by flow cytometry after two days of growth. K_B did not vary with the time of spent media extraction from the algae monocultures and K_B in algae spent media was only, on average, 46% lower than for fresh media (Figure S9B).

There Exists a Threshold light Level Below which Algae Cannot Suppress Bacterial Invasion

We performed an experiment to test the importance of light in the algal suppression of bacterial invasion. A culture of algae was grown in a flask (1 L) for ten days in a shaker incubator at approximately 4000 Lux, 30°C, and 175 rpm. The algae culture was then transferred to vials and inoculated with bacteria at bacterial density $2 \times 10^4 mL^{-1}$. These vials were placed in the temperature/light-control systems. In sets of two replicates the brightness was set to 600 Lux (extra low light) (Figure S8I), 1600 Lux (low light) (Figure S8J), 2900 Lux (medium light) (Figure S8K), and 4200 Lux (high light) (Figure S8L). Bacteria and algae abundance were then measured by flow cytometry.

Algae was only able to suppress bacterial invasion at the highest light level (Figure S8L). At all other light levels the bacteria invaded immediately. In contrast, in Figures 2H and 2J 1600 Lux monocultures of algae were able to suppress bacterial invasion as long as the algae density was high enough, whereas here, for example (Figure S8J), a 1600 Lux monoculture of high-density algae was not able to suppress bacterial invasion. This result implies that the physiology of algae grown in the flask in the shaker-incubator differs from algae grown in the temperature/light-control systems and that the suppression of bacterial growth by algae depends on the growth history of the algal culture or the culture conditions.

Hydrogen Peroxide Is Not Responsible for A Inhibiting B Invasion

Because metabolically active algae are known to produce reactive oxygen species (Roach et al., 2015), we tested if H_2O_2 was responsible for algae's ability to suppress bacterial invasion. To measure H_2O_2 we used the iodine based absorbance method of (Junglee et al., 2014). Absorbance values from cultures were compared to those taken for solutions with known concentrations of hydrogen peroxide.

In a control experiment we determined the concentration of H_2O_2 necessary to inhibit bacterial growth. Bacteria were inoculated into a 96-well plate in wells that contained 1/2x Taub .01% proteose peptone No. 3 and H_2O_2 in concentrations that ranged from 1 M to 1 nM. We inoculated bacteria at both $1 \times 10^4 mL^{-1}$ and $1 \times 10^5 mL^{-1}$. The bacteria were grown in a plate reader at 30°C and abundance was measured continuously via absorbance at 600 nm. For the low B inoculum, 1 mM initial H_2O_2 concentration was necessary to prevent growth while for the high B inoculum 10 mM initial H_2O_2 concentration was necessary to prevent growth. Measurements of H_2O_2 in these cultures one day after inoculation showed that bacteria who successfully grew eliminated the H_2O_2.

We then measured the H_2O_2 in conditions where B successfully invaded A and also conditions where its invasion was inhibited by A. Specifically, we took H_2O_2 measurements in the experiment from Figures S8I–S8L. No H_2O_2 was detected at any point in any of the systems, and thus we conclude that H_2O_2 is not the mechanism by which algae suppresses bacterial invasion. We cannot rule out other reactive oxygen species by this assay.

Algal-bacterial Adhesion and Invasion Supression

By closely examining flow cytometry data from the experiment in Figures S8I–S8L, it can be seen that bacteria are sticking to algae (Figure S10). Recall that in this experiment algae were grown in a flask for ten days and were then distributed across vials. These vials were inoculated with bacteria and then placed in the temperature/light-control systems at four different light levels. By looking at flow cytometry data taken 6 hours into the experiment, one can see that some of the bacteria have stuck to algae. This is evident from the presence of a small cloud of objects distinct from algal signals that are both high YFP and chlorophyll (Figures S10C and S10F).

We next asked: does the degree of bacteria sticking to algae depend on the degree to which the invasion is inhibited? In the experiment from Figures S8I–S8L, there were six immediately successful invasions and two suppressed invasions. We determined the density of the population of bacteria stuck to algae. For the six systems shown in Figures S8I–S8K where bacteria invade successfully immediately, we find that the fractional abundances of bacteria stuck to algae $\left(\frac{B - stuck - to - algae}{B - not - stuck - to - algae}\right)$ are: 3.7 ± 0.1%, 3.7 ± 0.1%, 2.8 ± 0.1%, 2.5 ± 0.1%, and 2.9 ± 0.1%. Error bars are estimated assuming Poisson counting error. For the two systems where

the invasions were suppressed (Figure S8L), we find 4.8 ± 0.9% and 7.7 ± 1.4%. A two-sample t-test assuming unequal variances fails to reject the null hypothesis that the average fraction of B cells stuck to A does not differ between successful and inhibited invasions ($p = 0.28$). We note the small samples size means this result should not be taken too seriously. However, based on the inconsistency between the two values in the case of the suppressed invasions, and the near-overlap between the error bars of one of the values for suppressed invasion (4.8 ± 0.9%), and two of the values for immediately successful invasion (both 3.7 ± 0.1%), we suggest it is not reasonable to believe that there is a substantially larger fraction of B adhered to A when B invasions are supressed.

Physical Collisions between Bacteria and Algae Are Frequent Even when Algal Density Is Low

In the main text we conjectured that the density dependence of algal inhibition of bacteria might arise from more frequent cell-to-cell contact when algal densities are high. Here we estimate the frequency of this contact and find that bacteria come in contact with algae with high frequency even at low algal densities.

We calculate the number of algae that a bacterium encounters in one second. From Seymour et al. (2017) $E_B = 4\pi N_A(D_A + D_B)(r_A + r_B)T$ where E_B is the number of algae a single bacterium encounters in time T, N_A is the concentration of algae, D_A and D_B are the diffusivity of algae and bacteria respectively, and r_A and r_B are the radii of algae and bacteria respectively. Taking T to be 1 second, we will attempt to calculate a lower bound on E_B, the number of algae a bacterium encounters in one second. For N_A, we use 500mL^{-1} (5×10^8 m^{-3}), the starting concentration of algae, and therefore the lower bound. From Stocker, $D_B = \frac{U^2\tau}{3}$ where U is the speed of the bacterium and τ is the turning rate. We take τ to be one turn per second (Hillen and Swan, 2016). In our systems, U is not the swimming speed, but rather the speed imparted on the bacterium through stirring. The stir-bar in the vial turns at 450 rpm and is of diameter 1.5 cm. Assuming that the average bacterium will move at the same speed as the point halfway along the radius of the stir-bar, we obtain speed 0.17 m s^{-1}. D_B is therefore .0096 $\frac{m^2}{s}$. We set $D_A = 0$ in the interest of establishing a lower bound. We take r_B to be 1 μm and r_A to be 1 μm. Taken together, we calculate $\frac{E_B}{T}$ to be 180 collisions per second. That is 180 algae encountered per second by a single bacterium.

Live-dead Staining Experiments

When gating on clouds of points of flow cytometry data, an assumption is made that the cells which are fluorescent are alive and thus a good measure of true abundance of live cells. We base this assumption on the fact that algae cells fluoresce significantly differently in chlorophyll when alive as compared to dead (Pouneva, 1997). Nevertheless, we attempt here to use Sytox Green Dye to assay the number of dead cells. Sytox Green is a nucleic acid stain that stains dead cells positively in the YFP channel.

We performed the Sytox experiment on algae in four cases, two replicates of a day 4, 1600 Lux (low light) ABC co-culture, and two replicates of a day 4, 4200 Lux (high light) ABC co-culture. In each case, flow cytometry data was taken before the application of Sytox (Figure S11A), then Sytox Green was added at a concentration of 100nM, incubated for 10 minutes, and then flow cytometry was performed again (Figure S11B). In each case, a new "dead algae" cloud with saturating YFP signal emerged after application of Sytox. Across the four cases, these dead cells made up 31 ± 11% of the total algae cells, suggesting up to a third of algal cells are dead. This estimate is likely to be an overestimate due to high stain concentrations.

Note what happens when a 5-fold higher Sytox concentration is used to stain algae (Figure S11C). The estimate of percentage of dead cells increases from 31 ± 11% to 51 ± 21% (average and standard deviation across four replicates). This increase indicates that we are in a regime of high Sytox concentration where even live cells are being stained with Sytox Green. Further supporting this conclusion is the fact that the main cloud of algae points in Figures S11B and S11C is also becoming distorted toward high YFP due to excess Sytox staining live cells.

The Sytox experiment was also performed on bacteria in four cases (but only with 500nM Sytox), two replicates of a day 14, 1600 Lux B monoculture, and two replicates of a day 14, 4200 Lux B monoculture. Once again a high YFP portion separated out from the main cloud after application of Sytox (Figures S11D and S11E). In the case of bacteria, dead cells made up 3.6± 2.1% of the total bacterial cells (average and standard deviation across four replicate systems). The Sytox experiment was also performed on ciliates, but the results are impossible to interpret given that Sytox just translated the entire cloud of ciliates to a higher YFP region (Figures S11F–S11H) and no separation is observed.

The Sytox Green staining protocol suggests performing repeated staining experiments at varying concentrations of dye and choosing the highest concentration where a subset of the presumably live cells are not stained. Further, the ability of cells to expel the dye depends on their physiological state (e.g. exponential versus stationary phase). Since this state varies throughout our experiment we deemed it infeasible to perform Sytox staining at many time points for the many different conditions studied here. However, the staining data we do have supports the claim for algae and bacteria that less than ~31 % of the algal population or ~5 % of the bacterial population are dead. We conclude that for bacteria the bulk of the population we measure by YFP fluorescence is alive. For the algae, while roughly 1/3 of cells may be dead this fraction is small relative to the 100-fold increase in density we observe over the course of growth.

Successful Bacterial Invasions Are not an Artifact of Mis-classifying Algae Detritus as Bacteria

Given that detritus accumulates over the course of experiments, we looked closer at flow cytometry data to confirm that accumulating algae detritus was not being mislabeled as a successfully invading bacterial population. First we plotted YFP signal versus SSC signal for time points at the beginning, middle, and end of a 1600 Lux (low light) algae monoculture. We then examined the number of objects as a function of time that lay within a gate typically used to count bacteria. Over the course of this algae monoculture, only a small number of objects (<100) lay within this gate. The same was true for a 4200 Lux (high light) algae monoculture. In contrast, there were approximately a thousand times as many objects in this gate at the end of a 1600 Lux B invasion on A and a 4200 Lux B invasion on A. These results suggest that algal detritus is not a strong contributor to the number of counts of B we observe by flow cytometry.

Modeling: Lotka-Volterra Model with Higher Order Interaction

The first model presented in Box 1 is a phenomenological model of abundance dynamics is given in Equations 1, 2 and 3. We note that the three-species term alone cannot account for bacteria-ciliate interactions in the absence of algae, therefore we model the predation of bacteria in the absence of algae using a competitive LV term of the form $1-\frac{x_B+\beta x_C}{K_B}$. While unrealistic given what we know about the system, this form is necessary since including a term $-Fx_Bx_C$ causes the presence of ciliates in any community to drive the bacteria extinct. This outcome is expected since the bacteria have no explicit defense against predation in this model. The competitive LV term acts to lower the carrying capacity of bacteria in the presence of ciliates providing an effective description of the fact that some bacteria can avoid predation and persist. We simulated this model and showed that it can recapitulate the dynamics we observe experimentally (Figure S13).

Modeling: Details of Model Including Bacterial Aggregation

Box 1 also shows a model of population dynamics in the ABC community that includes bacterial aggregation dynamics. The model captures the following experimental observations:

- Bacteria successfully invade AC communities with low algal densities
- Bacteria fail to invade AC communities when A is at high density
- Bacteria invade A and C monocultures with slower invasions of A monocultures at high A densities
- C induces B aggregation
- A inhibits B aggregation
- There is no competition for nutrients in the system that is responsible for these observations

In order to capture these features with a minimum of freely varying parameters, we constructed the model shown in Equations 4, 5, 6, 7, and 8. x_B is the density of planktonic (single-celled) bacteria, while A_B is the density of bacteria in aggregates. x_A and x_C are the density of algae and ciliates respectively. Note that the substrate which drives bacterial growth S is assumed unitless without loss of generality with an initial value of 1. Y then is the carrying capacity of bacteria in the medium used here ($3.9 \times 10^6 mL^{-1}$). Only planktonic bacterial cells (x_B) can grow on the substrate S. We assume that aggregated bacterial cells (A_B) do not grow since *E. coli* biofilms are known to exhibit a physiological state similar to stationary phase (Ito et al., 2008). Note that the model makes no claim on how many aggregates there are, nor how many bacteria make up a given aggregate; A_B simply denotes how many cells of bacteria are in an aggregated state. We then obtain the total number of bacterial cells $T_B = x_B + A_B$. T_B is what is plotted for bacterial abundances in all figures in the main text and is the output of our aggregate correction algorithm discussed above. Below we justify the functional forms used in this model and the parameter values we chose for numerical simulation.

The parameters of the model are described in Table S3 with their corresponding values. We are able to directly measure or use previous work to constrain all parameters except r_{AB}, α_1 and α_2. r_{AB} must be on the same order as r_B in order to observe substantial inhibition of B growth by A so we set this parameter accordingly. α_1 and α_2 are inferred indirectly from the data Table S3.

Bacteria-ciliate Interactions

To begin, we ignore the algae and examine the interaction between the bacteria and the ciliates. This interaction is characterized by five parameters: r_B, Y, α_1, F, r_C and K_C. Of these parameters, r_B, Y, r_C, K_C and F can be inferred from data acquired for this study. For a more detailed discussion of the estimate of F, the feeding rate, from our data, see below. This leaves α_1, the rate at which the ciliates induce B aggregation, unknown. We therefore performed simulations on a pair-culture of B and C while varying the parameter α_1 in order to see which value of α_1 best reproduces the data. The results of these simulations are shown in Figure S12. The simulations show an intuitive result. In all cases, the bacteria (T_B) grow to a high density before the ciliates (x_C) have grown to an appreciable density. The aggregation rate α_1 then determines how much the bacterial density crashes after that peak. If the aggregation rate α_1 is low, the bacteria fail to aggregate sufficiently quickly to avoid predation and the total bacterial density T_B crashes severely. Conversely, if α_1 is set high, bacteria aggregate quickly and avoid predation and experience only a very mild fall after the abundance peak. Typically in experiments when B is grown in coculture with C, we observe bacterial densities peaking to about $1 \times 10^6 mL^{-1}$ before dropping to about $1 \times 10^5 mL^{-1}$ (Figure 1H). Matching simulations to these values is one criteria for choosing α_1. The other criteria is as follows. In BC co-culture experiments we observe a transient spike (i.e. the peak followed by crash) in bacterial density

while in invasion experiments of B on C the bacterial density does not exhibit a spike (e.g. Figure 2). The absence of the spike in bacterial abundances in invasion experiments is likely due to increased initial bacterial aggregation in invasion experiments which is itself driven by the fact that the ciliates are at higher density at the time of bacterial introduction. Taking both criteria into account, we want the aggregation rate α_1 to be low enough that bacterial density drops to 1×10^5 mL^{-1} in BC co-culture simulations, but high enough that the bacteria do not exhibit a spike in B-invasion-of-C simulations (Figure S12, panel with red borders). We take $\alpha_1 = 2.5 \times 10^{-6}$ mL h^{-1}.

Predation Rates and Functional Form

Here we justify three modeling assumptions regarding the predator-prey interaction between C and B: (1) the functional response (B loss term) is linear in bacterial densities, (2) the feeding rate is estimated to be 1×10^{-5} mL h^{-1}, (3) the numerical response (growth of C due to predation on B) is negligible.

First, there is substantial evidence that the functional response of *T. thermophila* consuming bacterial prey is sigmoidal (e.g. $f_{max}x_Bx_C/(U + x_B)$ where f_{max} and U are constants). The typical justification for this is the presence of a prey handling time which limits the absolute rate at which a predator can consume a prey (Dawes and Souza, 2013). Measurements of C feeding rates as a function of bacterial density show clear saturation at higher bacterial densities (Seto and Tazaki, 1971). The sigmoidal dependence of ciliate uptake rates on prey concentration is further supported by studies of ciliate uptake of latex microspheres (Corno and Jürgens, 2006). These studies give a half-velocity constant (U) for the sigmoidal prey uptake rate in the case of *T. thermophila* of 10^7 bacteria mL^{-1}. Further studies show limited growth of *T. vorax* for *E. coli* densities below 2×10^7 mL^{-1} (Roach et al., 2015). We conclude that for our experiment, where bacterial densities never rise above 4×10^6mL^{-1}, the functional response is well approximated by a linear model ($x_B \ll U$). We therefore use the term Fx_Bx_C to describe the impact of C on the (planktonic) bacterial densities. In this linear model, following previous convention (Fenchel, 1980a) we refer to the feeding rate as the per ciliate uptake rate of bacteria at low bacterial densities e.g. $F = f_{max}/U$.

Second, we claim that the feeding rate of ciliates on bacteria (F) has a value of 1×10^{-5} mL h^{-1}. This claim is supported again by the literature. Fenchel estimated a feeding rate of *Tetrahymena* of approximately 10^{-5} mL h^{-1} (Fenchel, 1980b). Hatzis et al. measured uptake rates in *Tetrahymena* of fluorescently labeled 2.74 μm diameter latex beads (at low bead concentration) and found rates between 10^{-5} to 10^{-4} mL h^{-1} while noting substantial population level heterogeneity in bead uptake (Hatzis et al., 1993). We note that studies with passive particles (latex spheres) avoid possible artifacts from prey aggregation. In a follow-up study the same authors note that the fraction of feeding ciliates declines substantially from about 80 % to 20 % as the ciliates enter stationary phase (Hatzis et al., 1994). We neglect this time dependent feeding rate in favor of model simplicity. Finally, we can make crude estimates of this rate from our data as well. If we neglect aggregation and algae, the dynamics of bacteria are given by $\dot{x}_B/x_B = (r_B - Fx_C)$. We measure $r_B = 0.3$ h^{-1}. We note that the growing bacteria are limited in their maximum density due to predation, at the crossover point (when predation and growth are balanced) $r_B = Fx_C$, or $F = r_B/x_C$. If we assume that this crossover point occurs when $x_C \sim 1 \times 10^4$ mL^{-1} (and before bacteria have consumed all substrate) this gives an estimate of $F \approx 3 \times 10^{-5}$ mL h^{-1}, in good agreement with previous estimates. Due to the dependence of C feeding rates on growth state of the population and particle sizes, both of which are changing in our experiment as C enters stationary phase and B aggregates, we fixed the feeding rate on the lower end of the reported range: 1×10^{-5} mL h^{-1}. Note that this feeding rate only applies to planktonic bacteria, x_B. In order to replicate the inability of ciliates to eat aggregates of bacteria, there is no feeding of ciliates on aggregating bacteria A_B in the model.

Third, we claim that the numerical response of the predator in response to predation is negligible and we therefore make C abundance dynamics independent of x_B (Equations 3 and 7). The results of Seto and Tazaki (Seto and Tazaki, 1971) show no growth of *T. vorax* on *E. coli* when the abundance of the latter is below 2×10^7mL^{-1}. In fact, these authors estimate a ciliate yield of 4×10^4 bacteria/ciliate (e.g. one ciliate is produced from the consumption of 4×10^4 bacterial cells). Further, Curds and Cockburn (Curds and Cockburn, 1968) measure the dry weight of *T. pyriformis* to be 1.3×10^{-10} g cell^{-1} and the yield on bacteria (*Klebsiella aerogenes*) to be 50 % by dry weight. If we take the dry weight of *E. coli* to be 280 fg (bionumbers.hms.harvard.edu, BNID: 103904) we estimate approximately 1×10^3 bacteria/ciliate. Therefore, we expect the yield of C on B to be between 1×10^3 to 4×10^4 bacteria/ciliate. Our data show that C predation reduces bacterial abundances from approximately 1×10^6 to 1×10^5 mL^{-1} (Figure 1H, main text). Based on this reduction in B density, and the range of yields, we expect predation to produce between 50 and 1000 ciliates. Given the carrying capacity of C on this medium is 1.2×10^4 mL^{-1} we conclude that the numerical response generates at most 10 % of the maximum C population. Finally, when we compare abundance dynamics of C in the presence and absence of B we see no significant difference (Figures S9E and S9G).

Algae-Bacteria Interactions

Modeling AB interactions and dynamics requires two assumptions: (1) A growth rate depends only on light level and composition of the community, (2) A inhibits growth of B but not carrying capacity.

First, Table S1 shows measured growth rates of A as a function of light level and community composition. At low light, algal growth rate decreases substantially with the addition of B and/or C. At high light, to within the precision of our measurement, A growth rate does not depend on community composition. Rather than construct a functional form with its own parameters that relates algal growth rate to light and community composition, we simply set the algal growth rate for each combination of light level and community composition. Since the dynamics of B are the focus of our study, and A dynamics are always well described by a logistic model, this modeling choice is well justified and removes unnecessary parameters from our model.

Second, as shown in Equation 4, we assume that A impacts the growth rate of B in a density dependent fashion ($r_B S - r_{AB} x_A / K_A$), but also that A has no impact on the carrying capacity of B. Our data support this assumption since we see no impact of the presence of A on the carrying capacity of B. In the situation where B invades a high density (>1 × 10^5 mL^{-1}) algae culture, we find that the bacterial growth is strongly inhibited in about half of the cases we observed. We therefore capture this growth inhibition using the term shown above. We note that this purely deterministic model will not capture the stochastic outcomes we observe experimentally. We set r_{AB} to be on the same order as r_B. We make this assumption since our data clearly show that A is capable of nearly completely, or completely, inhibiting the growth of B (e.g. when $x_A = K_A$ near-complete inhibition will occur if $r_{AB} \approx r_B$).

Third, we must specify the unknown parameter α_2. To infer this parameter we make the following note about the model. If we assume, as is true late in the experiment, that the time derivatives are approximately zero then $\dot{A}_B = 0$ and we find $\alpha_2 = \frac{\alpha_1 x_B x_C}{A_B x_A}$. Examining the time series in Figure 2F we note that abundances are stable after ≈10 d. We compute α_2 via the fraction given above and the inferred value of α_1 and find a median value across all data points taken after 10 d to be $\alpha_2 = 7.7 \times 10^{-8}$mL h^{-1}. Note that to accomplish this we measure A_B using the clump correction algorithm described above. In all simulations shown in the main text we use this value. As a result our model has no free parameters.

Code for simulations of both models is available at: https://doi.org/10.13012/B2IDB-0946028_V1.

Aspects of the Dynamics Not Captured by the Model Including Bacterial Aggregation

The model presented here is necessarily simplified to limit the number of parameters. As a result there are several qualitative aspects of the data that are not captured by the modeling framework. Here we enumerate these.

- B exhibits a transient spike in aggregation as it enters stationary phase even in the absence of A or C. (e.g. Figure S1K). This process has been examined previously in our group and explained using a substrate dependent aggregation process (Merritt and Kuehn, 2016). We neglect this aspect of the bacterial aggregation dynamics.
- In co-culture conditions with B in the presence of C, after the peak in bacterial abundance and then subsequent fall due to predation, the abundances of B rise over the last ~10 days of the experiment. (Figure 6H). This rise could be explained by slow growth of aggregated bacteria or by growth of B on the detritus of dying C. Our model fails to capture the rise and we have not included it since we have no direct evidence for either of these processes.
- The deterministic ODE framework does not capture the stochasticity we observe in the outcome of B invading A alone (e.g. Figures S8C and S8D). This stochasticity could be captured by an effective randomness in the parameter r_{AB}. We have not included it here since the process is likely driven by population structure in either A or B which is not present in the current model (e.g. phenotypic heterogeneity in the response of B to inhibition by A). In the absence of direct mechanistic insight into this stochasticity process, we omitted it from our model.
- The decline in C abundances after approximately 4 days is not modeled here. This decline could be addressed by inferring a death rate from the data, but it would not qualitatively impact the agreement between the model and the simulation.

Simulations

Numerical integration of the model was performed using custom written Matlab scripts. Time steps of 1 minute were used to ensure numerical stability and accuracy. Organisms that fell below a density of 1 mL^{-1} were assumed extinct and could not recover. Invasions were accomplished by instantaneously adding a fixed density of B at t_{inv}.

QUANTIFICATION AND STATISTICAL ANALYSIS

Error Bars on Abundance Measurements by Flow Cytometry

Error bars on abundances are calculated by performing propagation of two forms of error: (1) the Poisson error inherent in counting a finite number of cells and (2) the uncertainty in volume run through the flow cytometer. The uncertainty in flow rate is taken as the standard deviation across the three replicates of bead calibration on the day the abundance was measured.

DATA AND CODE AVAILABILITY

Code for simulations and abundances measured by flow cytometry are available at: https://doi.org/10.13012/B2IDB-0946028_V1.

Cell Systems, Volume *9*

Supplemental Information

Higher-Order Interaction between Species Inhibits Bacterial Invasion of a Phototroph-Predator Microbial Community

Harry Mickalide and Seppe Kuehn

TABLE S1: Growth rates of A and C at 1600 Lux and 4200 Lux. Related to Figures 1 and 2.

Growth rate of A at 1600 Lux

Species Composition	Replicate	Growth R. [day^{-1}]	Error	Mean Growth R. [day^{-1}]	Error
A	1	1.13	0.13	1.08	0.07
	2	1.11	0.40		
	3	1.00	0.21		
AB	1	0.56	0.06	0.74	0.26
	2	0.93	0.11		
AC	1	0.71	0.04	0.61	0.10
	2	0.53	0.03		
	3	0.70	0.14		
	4	0.52	0.07		
ABC	1	0.44	0.06	0.39	0.07
	2	0.34	0.06		

Growth rate of A at 4200 Lux

Species Composition	Replicate	Growth R. [day^{-1}]	Error	Mean Growth R. [day^{-1}]	Error
A	1	1.92	0.91	1.76	0.19
	2	2.08	0.28		
AB	1	1.67	0.91		
	2	1.70	0.99		
AC	1	1.83	0.20		
	2	1.73	0.38		
ABC	1	1.65	0.83		
	2	1.47	0.87		

Growth rate of C at 1600 Lux

Species Composition	Replicate	Growth R. [day^{-1}]	Error	Mean Growth R. [day^{-1}]	Error
C	1	2.28	1.73	2.01	0.59
	2	2.48	9.92		
AC	1	1.01	0.25		
	2	2.34	12.72		
	3	3.04	0.51		
	4	1.71	1.42		
BC	1	2.01	3.89		
	2	2.22	3.42		
ABC	1	1.47	1.31		
	2	1.53	0.44		

Growth rate of C at 4200 Lux

Species Composition	Replicate	Growth R. [day^{-1}]	Error	Mean Growth R. [day^{-1}]	Error
C	1	1.54	2.18	1.43	0.39
	2	1.15	3.71		
AC	1	0.87	0.49		
	2	1.00	0.48		
BC	1	1.95	3.70		
	2	1.72	1.89		
ABC	1	1.39	1.56		
	2	1.80	3.07		

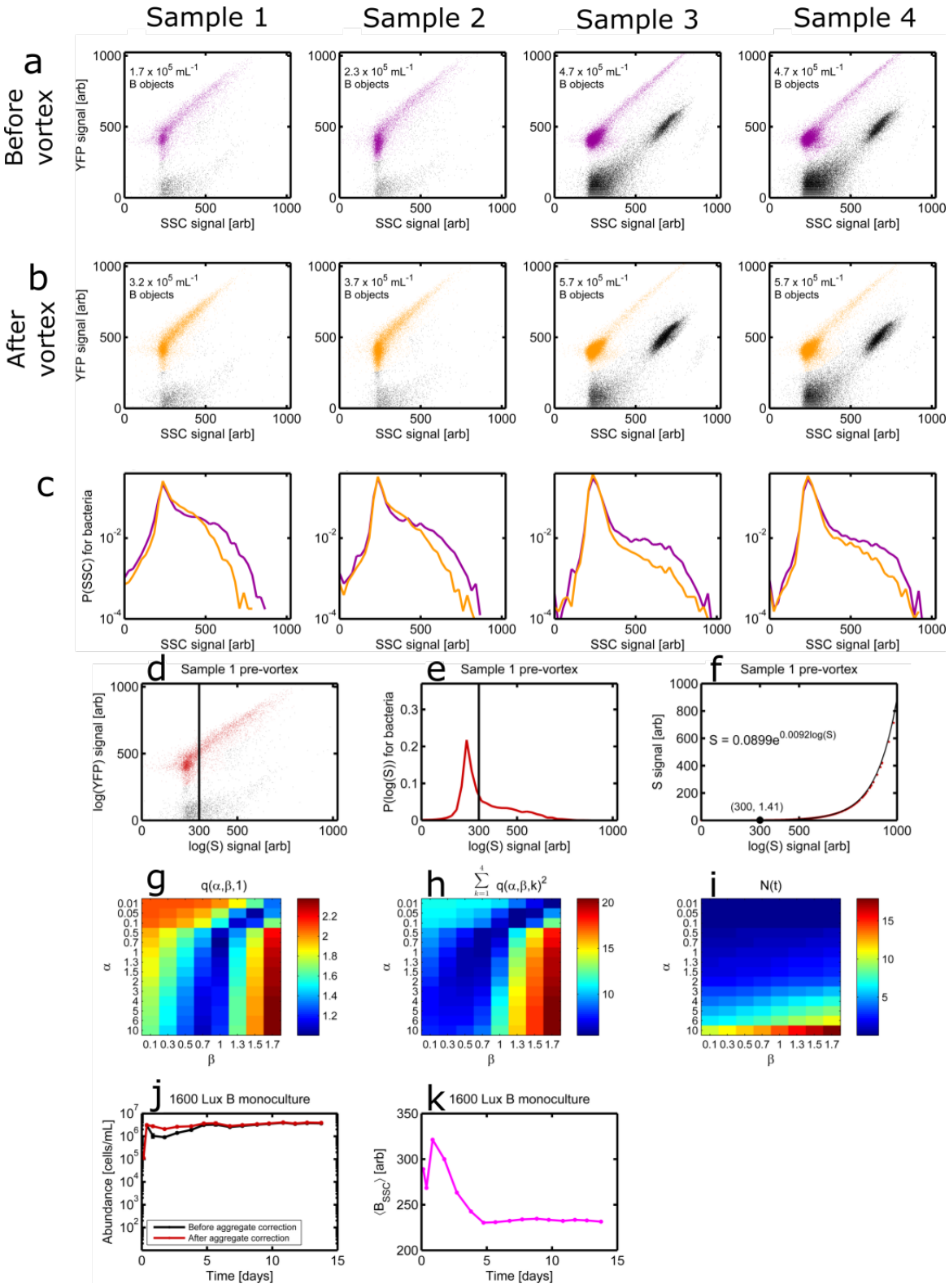

FIG. S1: **Vortex experiments shows high SSC objects are bacterial aggregates and aggregate correction algorithm corrects for aggregates. Related to STAR Methods. a,** Yellow fluorescence signal (YFP) plotted versus side-scatter signal (SSC) for flow cytometry data from day 12 of a 1600 Lux BC coculture (Samples 1 and 2) and a 1600 Lux ABC coculture (Samples 3 and 4). Points colored purple are classified as bacterial objects. The number reported in the plot indicates abundance of bacterial objects. **b,** Flow cytometry data from those same samples, but after vortexing. Points colored yellow are classified as bacterial objects. In all cases the abundance of objects classified as bacteria increases after vortexing. **c,** Overlays of histograms of side-scatter signal of bacterial objects from before and after vortexing. **d,** YFP plotted versus SSC for flow cytometry data for sample 1 prior to vortexing. Red points indicate objects we have labeled bacteria. The black line indicates the threshold between single cells and aggregates at $t = 300$. **e,** Histogram of $log(S_{i,p,1})$ signal for bacteria with the threshold indicated by the line. **f,** Plotting $S_{i,p,1}$ vs $log(S_{i,p,1})$ (red) with the fitted curve (black). The threshold is indicated by the black labeled point. **g,** A heat map of $q(\alpha, \beta, 1)$ where we have plotted $1/q$ when $q < 1$. **h,** A heatmap of $\sum_{k=1}^{4} q(\alpha, \beta, k)^2$ where again we take $1/q$ for values of α and β where $q < 1$. **i,** $N(S = 1.41)$ as a function of α and β (recall $t = 1.41$). **j,** Abundance dynamics for a 1600 Lux (low light) B monoculture before (black) and after (red) aggregate correction. **k,** Mean SSC (aggregation) plotted versus time for that same 1600 Lux B monoculture

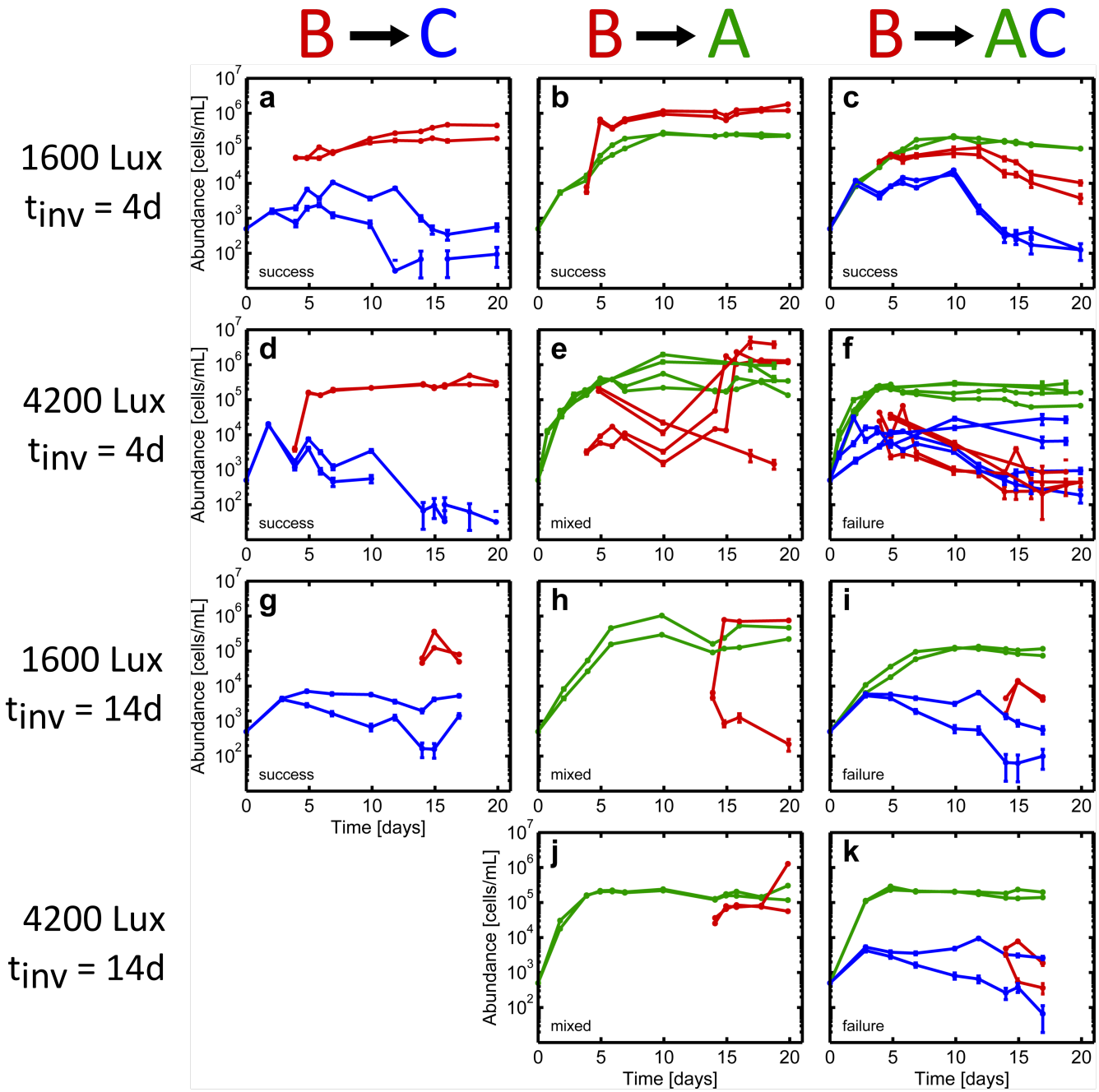

FIG. S2: **Figure 2 from the main text but without the aggregate correction algorithm applied** Panels are identical to Figure 2.

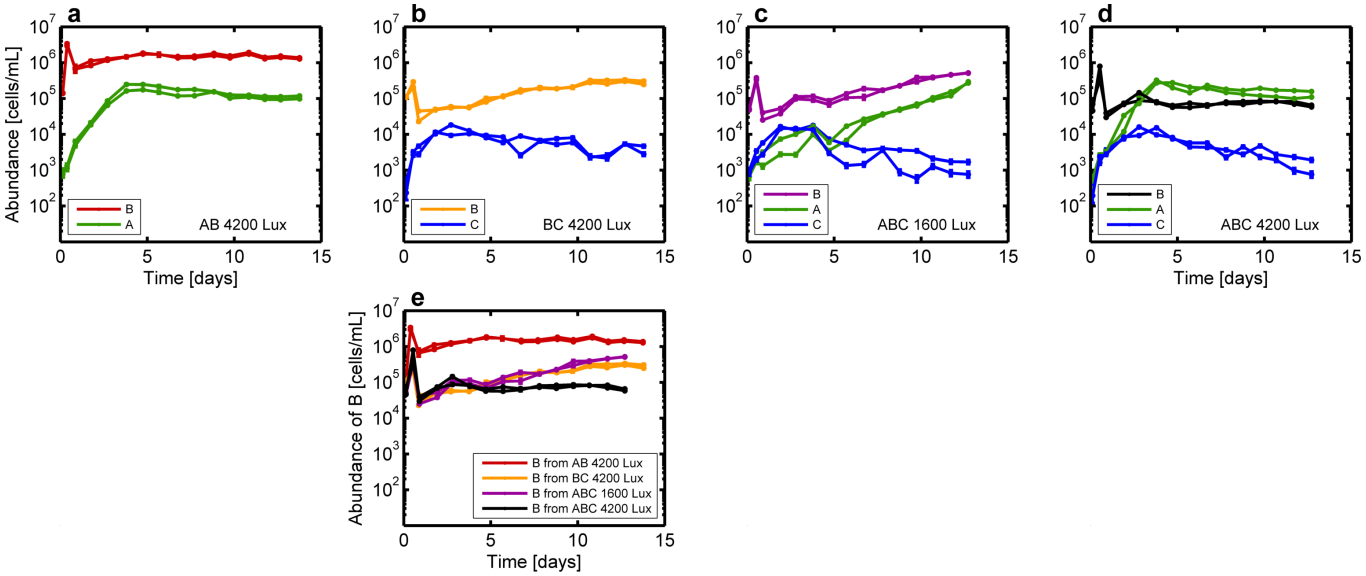

FIG. S3: **Figure 6 from the main text but without the aggregate correction algorithm applied** Panels are identical to Figure 6 of the main text.

Co-culture				
Light Level	Low	Low	High	High
A	7.06,6.85	7.13	6.04	6.46
B				
C	7.4	7.52	7.45	7.52
AB	7.16			
AC	7.72,8.6	8.45,8.67	8.31	8.28
BC	7.55	7.64	7.51	7.46
ABC	8.84	8.92	8.69	8.68
Day 14 B Invasion				
A	6.08	6.15	6.66	6.83
C	7.68			
AC	8.32	8.17	7.04	7.07
Day 10 B Invasion				
AC	6.65	8.02		
Day 4 B Invasion				
A	6.76	6.87	6.67	6.44
C	7.51	7.56	7.52	7.54
AC	8.44	8.17	6.52	6.76

TABLE S2: **Measurements of pH at the end of co-culture and invasion experiments. Related to Figure 1, 2 and 6.** Values correspond to pH measurements at the end of the respective time series shown in Figure 1, 2 or 6 of the main text. Omitted values are experiments where pH was not measured at the end. For invasion experiments numbers in red indicate failed B invasions as defined in the main text and green indicates successful invasions. The 10 day B invasion of AC time series is not shown in the main text but is included for completeness.

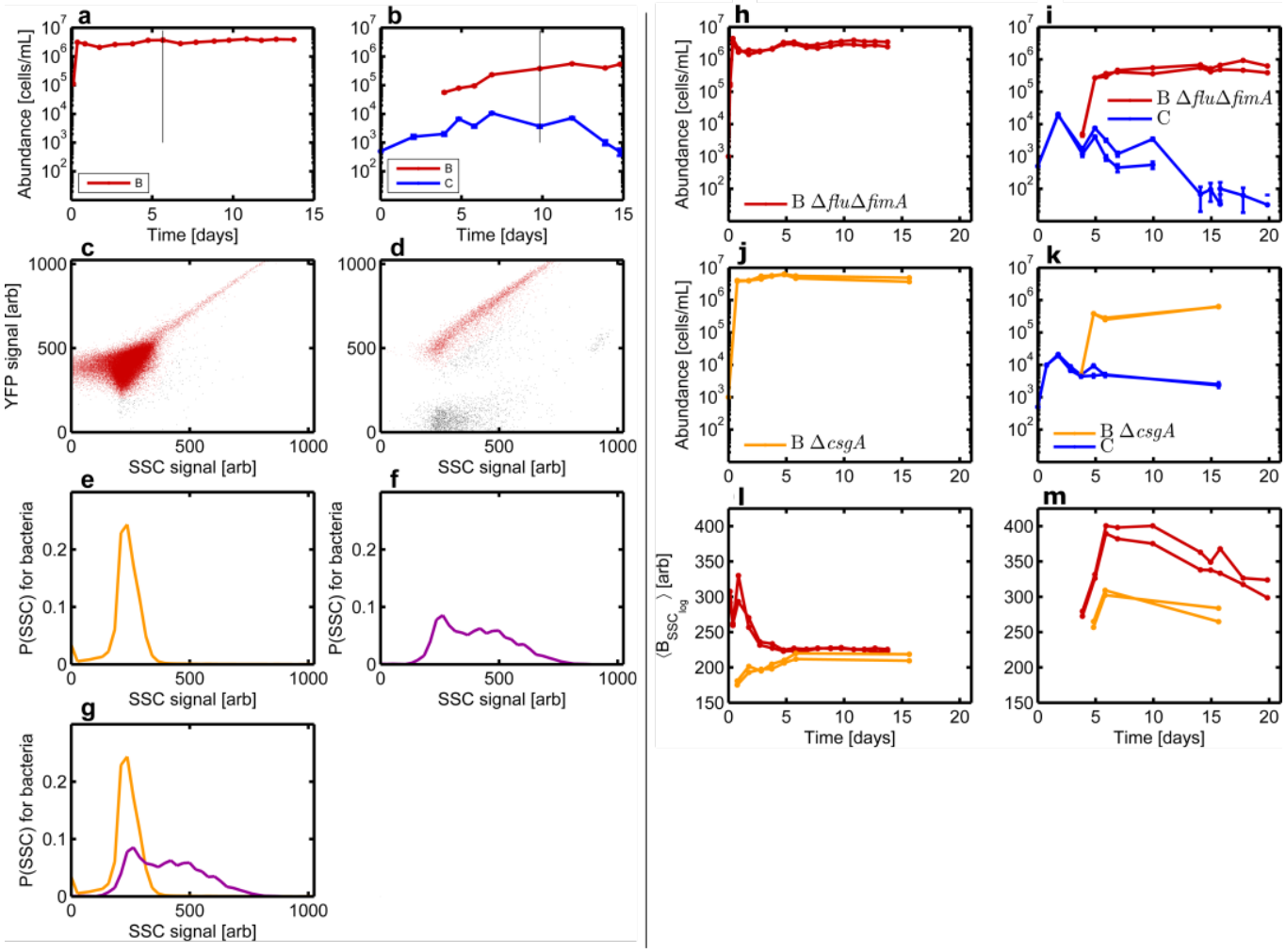

FIG. S4: **Ciliates induce bacteria to aggregate. Related to Figure 5. a,** Abundance dynamics for a 1600 Lux (low light) monoculture of B. Black line indicates the time point for which we plot flow cytometry data in **c. b,** Abundance dynamics for a 1600 Lux (low light) B invasion of C. The black line indicates the time point for which we plot flow cytometry data in **d. c,d** Plotting yellow fluorescence (YFP) versus side-scatter (SSC) for flow cytometry data taken from the indicated day in **a** and **b** respectively. Red-colored points indicate objects we have labeled as bacteria. **e,f**, Histograms of the SSC signal for all objects labeled as bacteria in **c** or **d**. **g,** Overlay of the histograms. All experiments in the following panels are at 4200 Lux (high light). **h,** Abundance dynamics for two replicates of a B monoculture, using strain $\Delta flu\Delta fimA$. This is the strain used throughout this study. **i,** Abundance dynamics for two replicates of a B invasion on C, also using the $\Delta flu\Delta fimA$ strain of B. **j,** Abundance dynamics for two replicates of a B monoculture, using strain $\Delta csgA$. **k,** Abundance dynamics for two replicates of a B invasion on C, also using the $\Delta csgA$ strain of B. **l,** Mean side-scatter plotted versus time for the bacteria in panels **h** and **j**. **m,** Mean side-scatter plotted versus time for the bacteria in panels **i** and **k**.

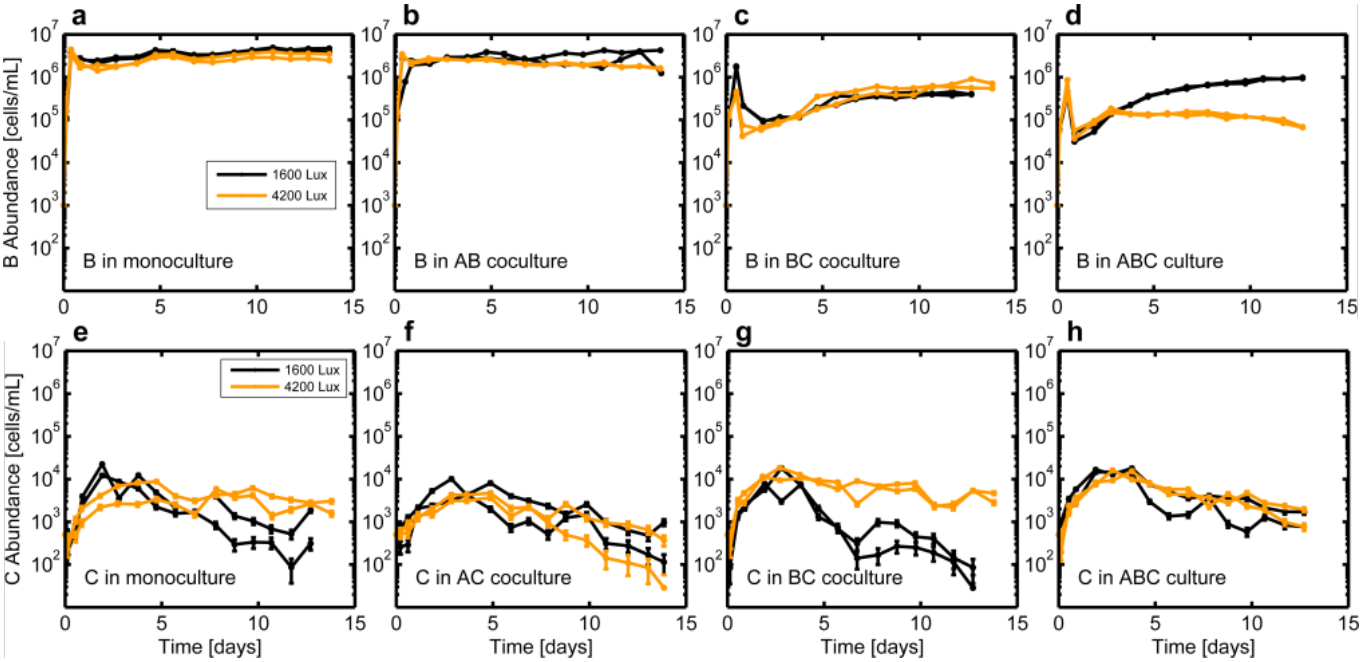

FIG. S5: **Bacterial or ciliate abundance dynamics with different light levels and community composition. Related to Figure 2. a-d,** Abundance dynamics for two replicates each of B in 1600 Lux and in 4200 Lux B monoculture (**a**), AB co-culture (**b**), BC co-culture (**c**), and ABC culture (**d**). Legend in **a** applies to **b-d**. **e-h,** Abundance dynamics for two replicates each of C in 1600 Lux and in 4200 Lux C monoculture (**e**), AC co-culture (**f**), BC co-culture (**g**), and ABC co-culture (**h**). Legend in **e** applies to **f-h**.

TABLE S3: Model parameter values. Related to Figures 2 and 6.

Parameter	Value	Source
r_B	$0.3\,\mathrm{h}^{-1}$	This study
r_{AB}	$0.29\,\mathrm{h}^{-1}$	Inferred
r_C	$0.073\,\mathrm{h}^{-1}$	This study
r_A (high light)	$0.073\,\mathrm{h}^{-1}$	Table S1
r_A (low light, w/BC)	$0.016\,\mathrm{h}^{-1}$	Table S1
r_A (low light, w/C)	$0.025\,\mathrm{h}^{-1}$	Table S1
r_A (low light, w/B)	$0.031\,\mathrm{h}^{-1}$	Table S1
r_A (low light, alone)	$0.045\,\mathrm{h}^{-1}$	Table S1
K_A	$2.3 \times 10^5 \mathrm{mL}^{-1}$	This study
K_C	$1.2 \times 10^4 \mathrm{mL}^{-1}$	This study
Y	$3.9 \times 10^6 \mathrm{mL}^{-1}$	This study
F	1×10^{-5} mL h^{-1}	[28][39][40], Inferred
α_1	2.5×10^{-6} mL h^{-1}	This study
α_2	7.7×10^{-8} mL h^{-1}	This study

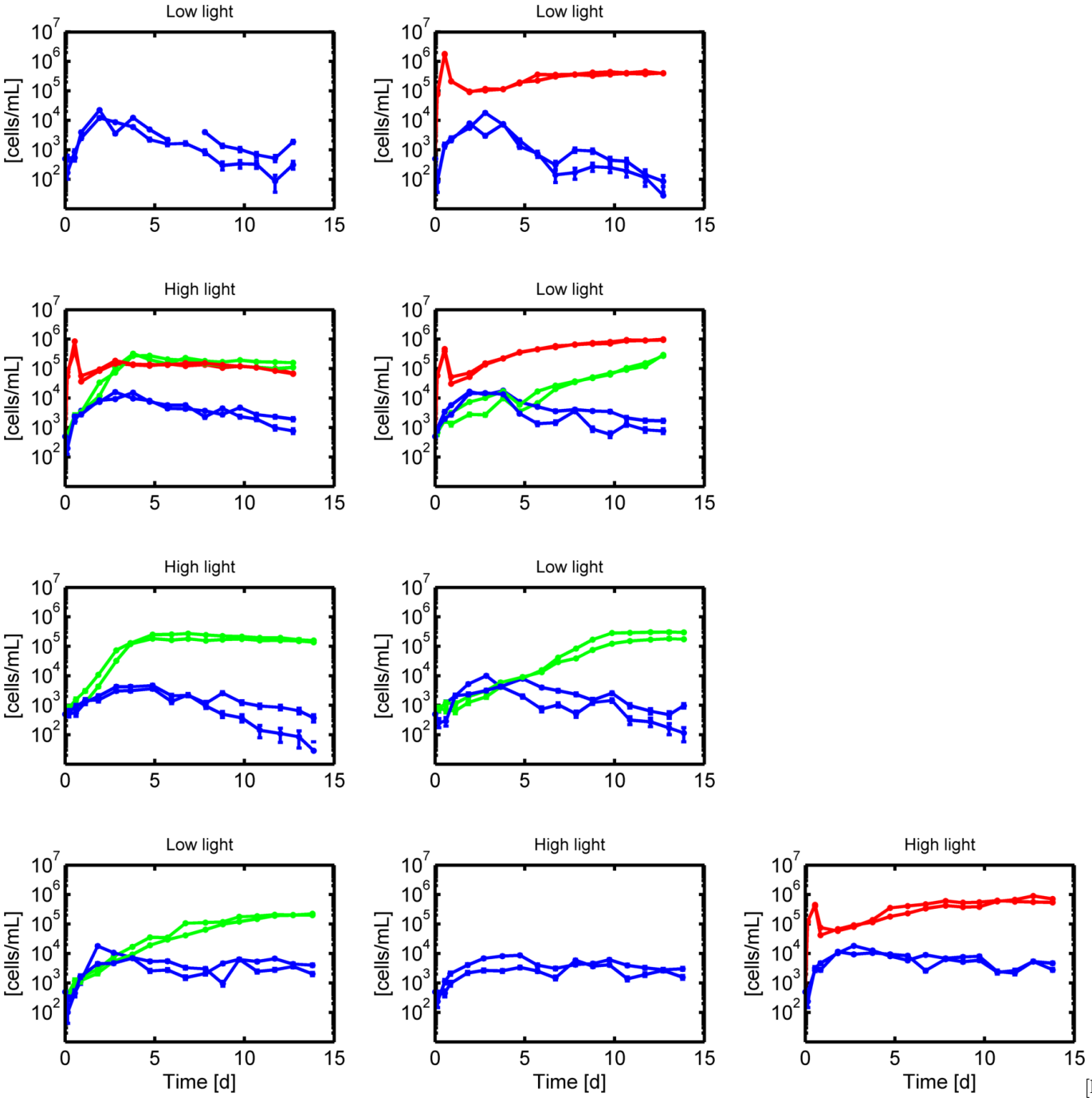

[h!]

FIG. S6: **Culture history is a strong determinant of C abundance dynamics. Related to Figure 2.**. A collection of abundance dynamics measurements for C across light levels and community composition. Each row of panels shows data for communities containing C which originated from the same pre-culture. Colors indicate species (A, green; B, red; C, blue). Light levels are given in the title of each panel. Note the similarity of C abundance dynamics for populations derived from the same culture (row).

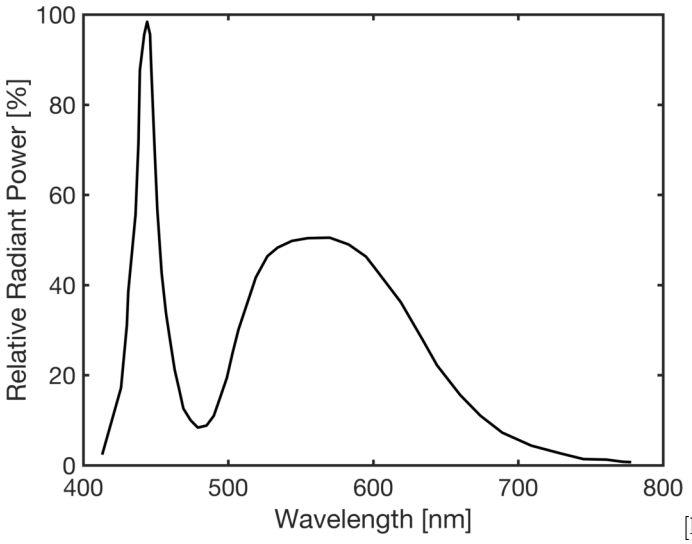

[h!]

FIG. S7: **Spectrum of the light LED light sources used in this study. Related to STAR Methods.** We used XP-L2 Cree LEDs with a color temperature of 4000K. The spectrum for these LEDs was not available, but the Cree XM series LEDs use the same die and are therefore expected to have the same spectrum. We digitized he neutral white spectrum from the Cree datasheet for the XM series LEDs and the result is shown in this plot. For the relevant datasheet see: https://www.cree.com/led-components/media/documents/XLampXML2.pdf green curve page 5. We did not measure the spectra of our LEDs directly.

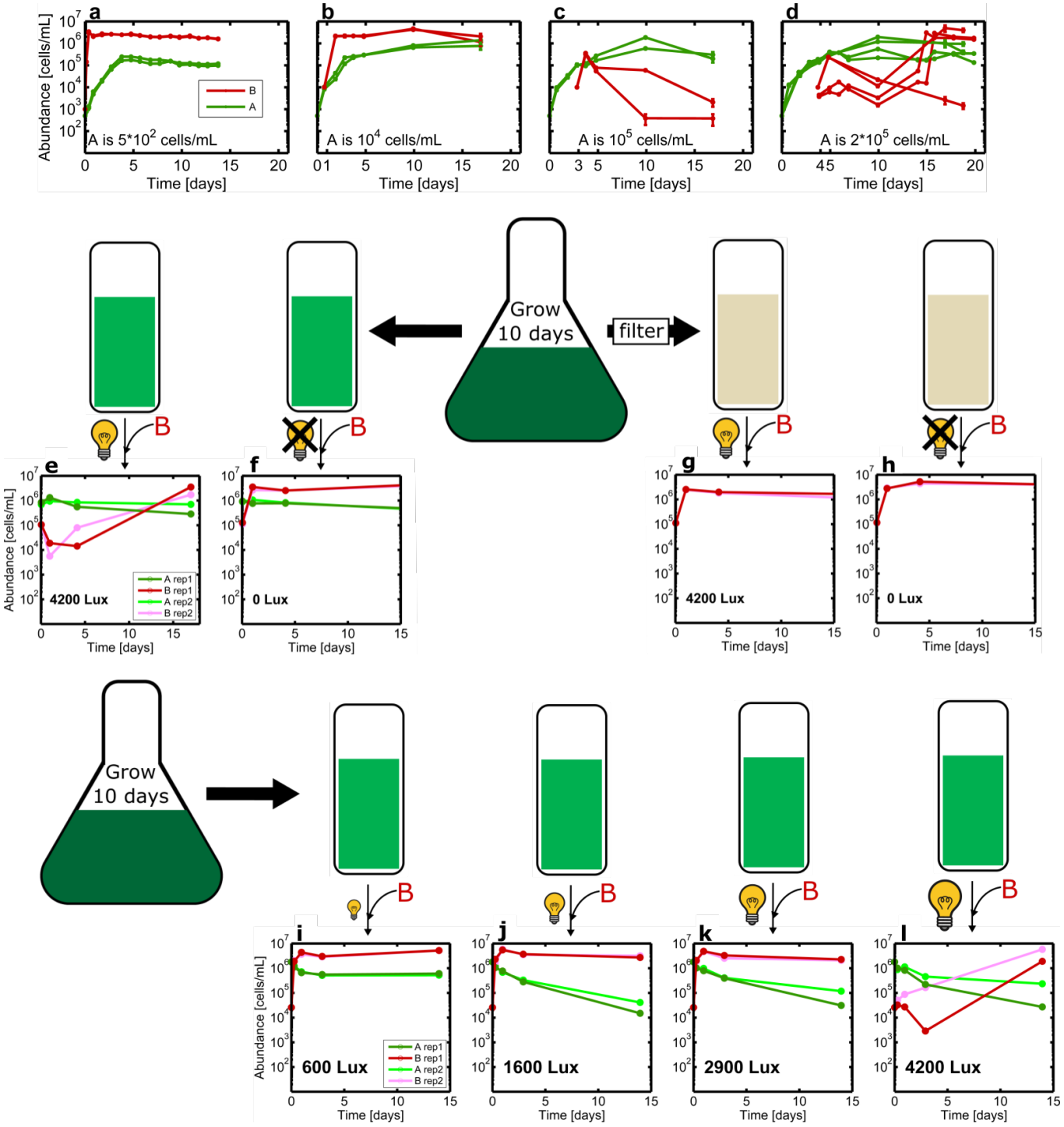

FIG. S8: **Experiments aimed at understanding algae-bacteria interactions. Related to Figures 3 and 4. a-d**, Abundance dynamics of algae and bacteria when bacteria is grown in co-culture with algae (**a**), or introduced into an algae monoculture at day 1 (**b**), day 3 (**c**), or day 4 (**d**). Text inside panels indicates density of algae at time of introduction of bacteria. All experiments in (**a-d**) performed at 4200 Lux (high light). **e-h**, Algae are grown for 10 days in large volume in a flask of 1/2xTaub .01%pp3 at 30 °C in a shaker-incubator while being illuminated at approximately 4000 Lux. Half the culture is filtered. Then unfiltered (**e,f**) and filtered (**g,h**) algae culture is distributed across vials. Bacteria is inoculated at density 1×10^5 mL^{-1} and the vials are then grown at 4200 Lux (high light) (**e,g**) or 0 Lux (no light) (**f,h**). Abundance dynamics after inoculation with bacteria are plotted. There are two replicates for each condition. **i-l,** Algae are grown for 10 days in large volume in a flask of 1/2xTaub .01% proteose peptone No.3 at 30 °C in a shaker incubator while being illuminated at approximately 4000 Lux. Algae culture is then distributed across vials. Bacteria is inoculated at density 2×10^4 mL^{-1} and the vials are then grown at 600 Lux (extra low light) (**i**), 1600 Lux (low light) (**j**), 2900 Lux (medium light) (**k**), or 4200 Lux (high light) (**l**). Abundance dynamics after inoculation with bacteria are plotted. There are two replicates for each condition.

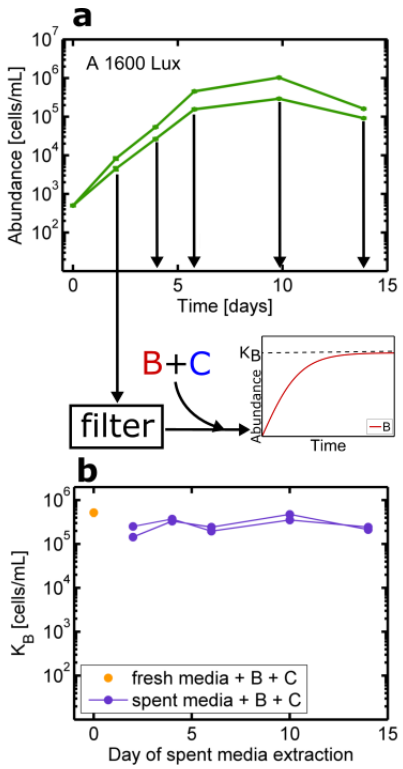

FIG. S9: **Additional spent media experiments. Related to Figure 3. a** Abundance plotted versus time for two replicates of an algae monoculture at 1600 Lux (low light). Black arrows indicate the time points at which media is extracted and filtered. Bacteria and ciliates are then grown together on this spent media in a microtiter plate, allowing B to reach saturating density K_B. **b** K_B, measured by flow cytometry, is plotted versus time of spent media extraction from experiment in panel (**a**). The fact that B reaches high density in the presence of C even in algal spent medium suggests that algae must be present to enhance ciliate predation rates on B.

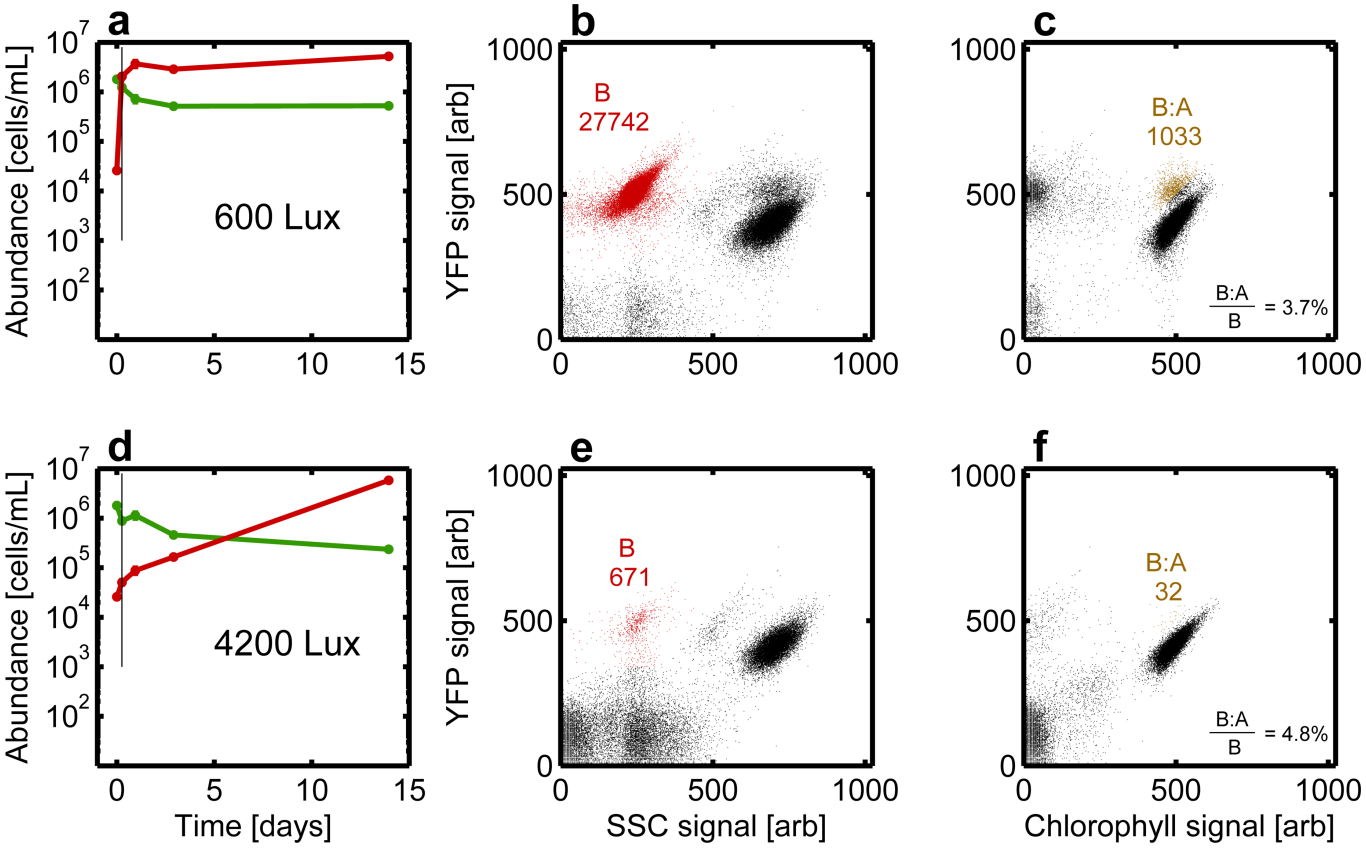

FIG. S10: **A small fraction of bacteria adhere to algae. Related to Figure 2-4. a,** Abundance curves for algae and bacteria taken from one of the 600 Lux replicates of the algae flask experiment in Fig. S8. The black line marks the time point for which flow cytometry data is plotted in **b&c. b,** YFP signal plotted versus SSC signal for flow cytometry data from aforementioned timepoint. Points in red mark objects classified as bacteria. Number indicates the number of these objects. **c,** YFP signal plotted versus Chlorophyll signal for flow cytometry data from that same timepoint. Points in gold mark objects classified as algae with bacteria stuck to them. Number indicates the number of these objects. Percentage indicates how many of these algae-stuck-to-bacteria objects there are as a fraction of the normal bacteria. **d,e&f,** The same analysis as in the top row of this figure, but instead with one of the 4200 Lux replicates from Fig. S8.

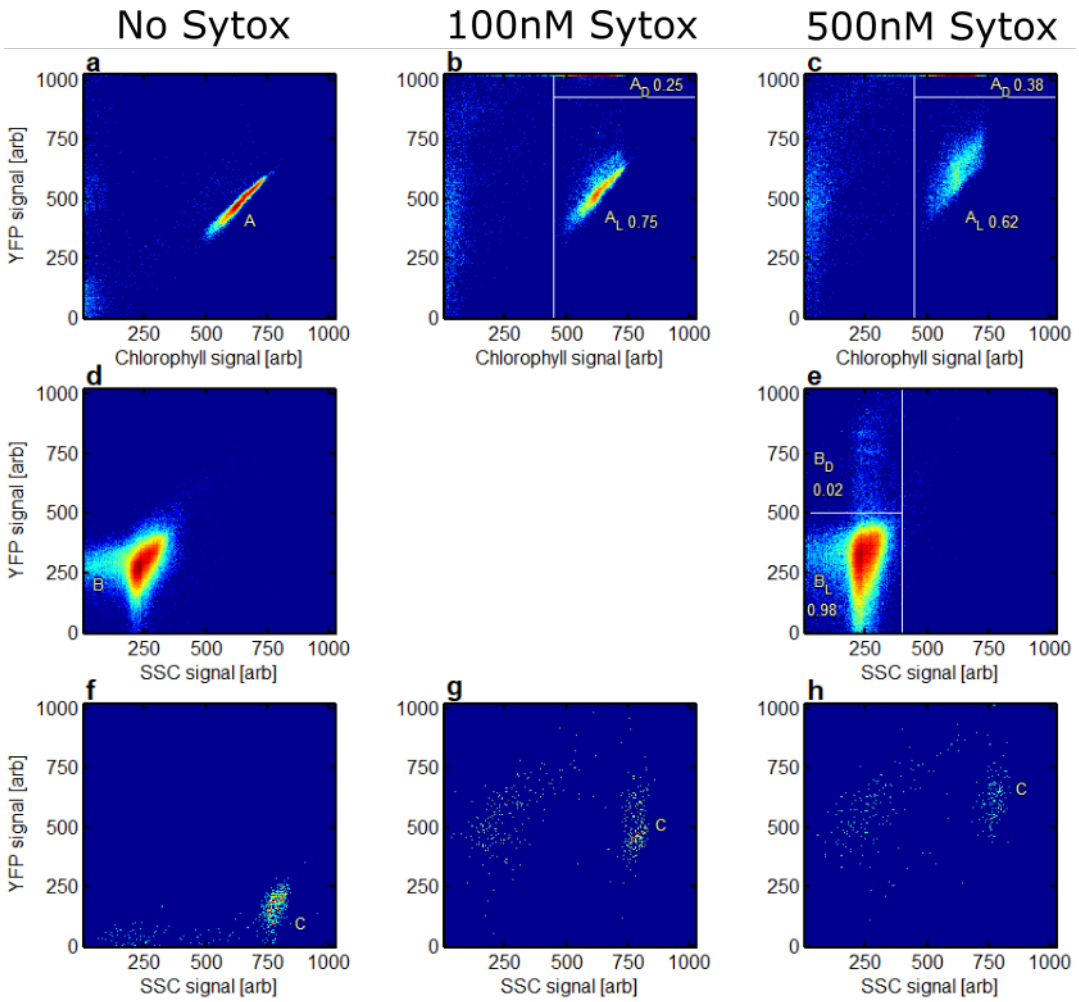

FIG. S11: **Live-dead staining of algae, bacteria, and ciliates. Related to Figure 1. a,** YFP signal plotted versus Chlorophyll signal for flow cytometry data taken from day 4 of a 4200 Lux ABC coculture. The cloud labeled A is known to be algae **b,** YFP signal plotted versus Chlorophyll signal for that same sample but after the application of 100 nM Sytox. At sufficiently low concentration, Sytox selectively increases the YFP signal of dead cells. Note how a cloud with saturating YFP signal, thought to be dead algae A_D, has separated from the main cloud of live algae A_L. Numbers indicate fraction of counts within corresponding white rectangle divided by total counts across both white rectangles. **c,** Same sample and analysis as panel **b** except in this case 500 nM Sytox has been used. Note how the additional Sytox significantly changes the ratio between live and dead cells. **d,e** A similar analysis is performed on bacteria by plotting YFP signal versus SSC signal. In this case, the sample is taken from day 14 of a 4200 Lux B monoculture and in panel (**e**) 500 nM Sytox is used. There is no data for 100nM Sytox on bacteria. **f-h,** A similar analysis is performed on ciliates. In this case, the sample is taken from day 4 of a 1600 Lux C monoculture. Unstained cells are shown in (**f**) and cells stained with 100 and 500 nM Sytox in panels (**g**) and (**h**) respectively. Note how at both Sytox concentrations, the entire ciliate cloud shifts in YFP rather than separating out into high YFP and low YFP clouds, thus making quantification of dead cells impossible.

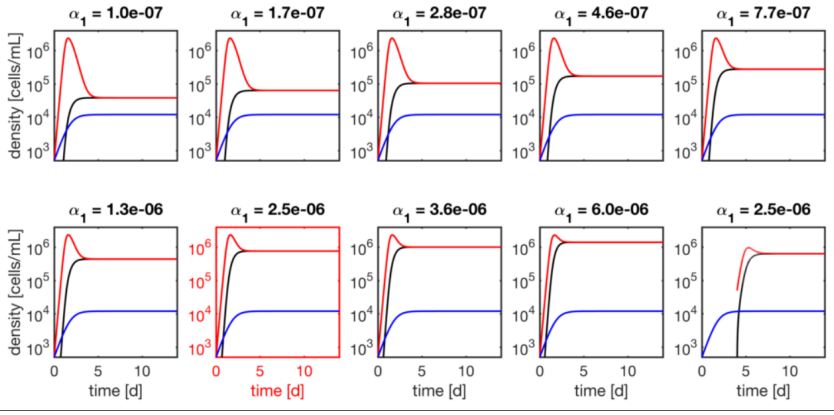

FIG. S12: **Determining α_1. Related to Figure 2,6.** In each panel x_C in blue, T_B in red, and A_B in black. Abundance dynamics of B and C in co-culture simulated using the model discussed above. Parameter values are as shown in Table S3 with the exception of α_1 which is varied as indicated in the title of each panel (units are mL h^{-1}). The bottom right panel shows abundance dynamics of B and C in invasion rather than co-culture. The red line and black line overlap at long times ($T_B = A_B$) because the ciliates eventually induce all bacteria to aggregate.

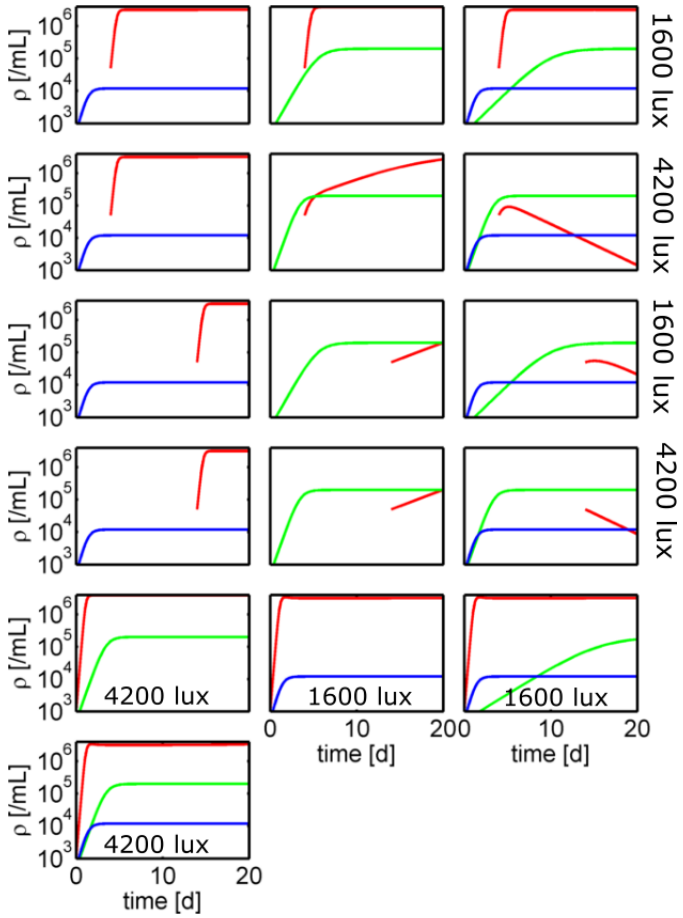

FIG. S13: **Phenomenological model with higher order interaction. Related to Figures 2 and 6.** Simulations of Lotka-Volterra model (see Box 1 main text). Parameters are identical to Table S3 with the following additions: $\beta = 60$, $r_{ABC} = 0.025\,h^{-1}$, $K_{AC} = K_A K_C$. Light levels for the first four rows are shown at the right and for the last four panels on each panel.